Available online at www.sciencedirect.com
ScienceDirect
Composites: Part B 39 (2008) 933–961
composites Part B: engineering
www.elsevier.com/locate/compositesb

Effects of particle size, particle/matrix interface adhesion and particle loading on mechanical properties of particulate–polymer composites

Shao-Yun Fu [a,*], Xi-Qiao Feng [b], Bernd Lauke [c], Yiu-Wing Mai [d,*]

[a] Technical Institute of Physics and Chemistry, Chinese Academy of Sciences, Beijing 100080, China
[b] FML, Department of Engineering Mechanics, Tsinghua University, Beijing 100084, China
[c] Leibniz-Institute of Polymer Research, Hohe Strasse 6, D-01069 Dresden, Germany
[d] Center for Advanced Materials Technology (CAMT), School of Aerospace, Mechanical and Mechatronic Engineering J07, The University of Sydney, Sydney, NSW 2006, Australia

Received 12 December 2007; accepted 7 January 2008
Available online 26 January 2008

Abstract

There have been a number of review papers on layered silicate and carbon nanotube reinforced polymer nanocomposites, in which the fillers have high aspect ratios. Particulate–polymer nanocomposites containing fillers with small aspect ratios are also an important class of polymer composites. However, they have been apparently overlooked. Thus, in this paper, detailed discussions on the effects of particle size, particle/matrix interface adhesion and particle loading on the stiffness, strength and toughness of such particulate–polymer composites are reviewed. To develop high performance particulate composites, it is necessary to have some basic understanding of the stiffening, strengthening and toughening mechanisms of these composites. A critical evaluation of published experimental results in comparison with theoretical models is given.

Keywords: A. Polymer–matrix composites (PMCs); A. Particle-reinforcement; B. Mechanical properties

1. Introduction

To cope with the obvious limitations of polymers, for example, low stiffness and low strength, and to expand their applications in different sectors, inorganic particulate fillers, such as micro-/nano-SiO_2, glass, Al_2O_3, $Mg(OH)_2$ and $CaCO_3$ particles, carbon nanotubes and layered silicates, are often added to process polymer composites, which normally combine the advantages of their constituent phases. Particulate fillers modify the physical and mechanical properties of polymers in many ways. This review is concerned with the latter properties, which are stiffness, strength and fracture toughness. The manufacturing processes and techniques for such particulate–polymer composites are, however, not covered here.

It has been shown that dramatic improvements in mechanical properties can be achieved by incorporation of a few weight percentages (wt%) of inorganic exfoliated clay minerals consisting of layered silicates in polymer matrices [1–12]. Commonly used layered silicates have a thickness of ~1 nm and lateral dimensions of ~30 nm to several microns or larger. The large aspect ratios of layered silicates are thought to be mainly responsible for the enhanced mechanical properties of particulate–polymer nanocomposites. There have been many papers on layered silicate reinforced polymer composites including some reviews [1,2,13, and references therein] and hence the case

* Corresponding authors. Tel./fax: +86 10 82543752 (S.-Y. Fu), tel.: +61 2 9351 2290; fax: +61 2 9351 3760 (Y.-W. Mai).
E-mail addresses: syfu@mail.ipc.ac.cn (S.-Y. Fu), y.mai@usyd.edu.au (Y.-W. Mai).

1359-8368/$ - see front matter © 2008 Elsevier Ltd. All rights reserved.
doi:10.1016/j.compositesb.2008.01.002

Nomenclature

a, b, c and d	constants in Eqs. (18) and (23)
A_1 and B_1	constants in Eq. (3)
B	empirical constant
C_1 and C_2	constants for a given composite
d_p	particle diameter
D_s	average interparticle distance
E_c	composite Young's modulus
E_m	matrix Young's modulus
E_p	particle Young's modulus
f	particle/matrix friction coefficient
f_c	a factor of phase morphology varying between 0 and 1
$F(d_p)$	parameter as a function of d_p and $0 \leqslant F(d_p) \leqslant 1$
g	constant
G_c	composite fracture toughness, also critical energy release rate
G_m	matrix fracture toughness, also critical energy release rate
k, H	constants in Eq. (26)
k_E	Einstein coefficient
$k(V_p)$	slope of the tensile strength against d_p
$k_p(V_p)$	constant as a function of particle volume fraction
k_ϕ	enhanced fracture surface volume fraction
K_c	composite fracture toughness, also stress intensity factor
n	parameter for G_c taking into account the extra fracture path around the particles
n_p	a parameter related to particle size and particle volume fraction
p	pressure
P	particle aspect (length to width) ratio
Q	parameter accounting for weaknesses in the composite structure caused by the discontinuities in stress transfer
s	crowding factor for the ratio of the apparent volume occupied by the particle to its own true volume and its value is between 1.0 and 2.0
S	constant in Eq. (30a)
S_r	strength reduction factor
T	line tension
V_p	particle volume fraction
$V_{p\,max}$	maximum packing fraction
$\widetilde{K}_c$	composite bulk modulus
W_c	impact toughness (work of fracture) of the composite, notched specimen
$\widetilde{K}_m$	matrix bulk modulus
$\widetilde{K}_p$	particle bulk modulus
$\widetilde{G}_c$	composite shear modulus
$\widetilde{G}_m$	matrix shear modulus
$\widetilde{G}_p$	particle shear modulus
α	particle/matrix adhesion coefficient
σ_c	composite strength or yield strength
σ_m	matrix strength
σ_a	particle/matrix adhesion strength
δ	E_p/E_m
χ_p	particle strengthening factor
ν_m	matrix Poisson ratio

of layered nanoparticles will not be discussed here. In contrast, much attention has been paid to carbon nanotubes (CNTs) as reinforcing fillers for polymers. There are many research papers and several reviews on the mechanical properties of CNT reinforced polymer nanocomposites [13–15, and cited references]. Improvements in mechanical properties have been observed by adding a few wt% of CNTs. In these studies, both layered silicates and CNTs have high aspect ratios.

Polymer composites containing particles with a small aspect ratio of 1 or thereabout have also been studied extensively because of their technological and scientific importance. Many studies have been conducted on the mechanical properties of these particulate-filled polymer composites. Stiffness or Young's modulus can be readily improved by adding either micro- or nano-particles since rigid inorganic particles generally have a much higher stiffness than polymer matrices [16–24]. However, strength strongly depends on the stress transfer between the particles and the matrix. For well-bonded particles, the applied stress can be effectively transferred to the particles from the matrix [25]; this clearly improves the strength [16,26–30]. However, for poorly bonded micro-particles, strength reductions occur by adding particles [17–19,31–37]. The drawback of thermosetting resins is their poor resistance to crack growth [38–41]. But inorganic particles have been found to be effective tougheners for thermosetting resins [22,42,43]. Though they do not increase the toughness as dramatically as rubber particle inclusions [44,45], they increase the elastic modulus and hardness much better than rubber particles. In contrast, most studies on thermoplastics filled with rigid particulates reported a significant decrease of fracture toughness compared to the neat polymers [19,35,46–48]. There are, however, several studies that show toughness increase with introduction of rigid particles in polypropylene [49,50] and polyethylene [50–57]. Impressively enhanced impact toughness has been reported for polyethylene filled with calcium carbonate particles by Fu and Wang [53–56] and Bartczak et al. [57]. Enhancement of impact properties of some pseudo-ductile polymers by the introduction of inorganic particles has also been achieved [57,58].

The mechanical properties of particulate–polymer composites depend strongly on the particle size, particle–matrix interface adhesion and particle loading. Particle size has an obvious effect on these mechanical properties. For example, smaller calcium carbonate particles provide higher strength of filled polypropylene composites at a given particle loading [14]. Sumita et al. [58] underlined the interest of replacing microscale silica by its nanoscale counterpart, since nanoscale silica particles possess superior mechanical properties. They found that these nanoparticles give higher rigidity and superior yield strength to the polymers. Smaller particle size yields higher fracture toughness for calcium carbonate filled high density polyethylene (HDPE) [57]. Similarly, alumina trihydrate filled epoxy containing smaller particles show higher fracture toughness [21]. Particle–matrix interface adhesion and particle loading are two important factors that also affect mechanical properties. For example, the tensile strength of glass bead filled polystyrene composites depends on the particle–matrix adhesion and increases with it [17]. Thus, the use of coupling agents that increase the particle–matrix adhesion leads to higher strength [22,38,42,59–62]. When chemical treatment was applied to the silica particles in HDPE, the toughness of the filled polymer was significantly improved [46]. The strength of polyimide/silica composites increases with particle loading to 10 wt% [16] and decreases beyond that. However, their modulus increases monotonically with silica particle loading [16]. Moreover, the fracture toughness of glass bead filled epoxy composites increases initially with increasing filler loading till a plateau value is reached at a critical particle volume fraction [63].

From the preceding paragraphs, it is clear that the mechanical properties of particulate-filled polymer micro- and nano-composites are affected by particle size, particle content and particle/matrix interfacial adhesion. This review will focus on how these factors influence the mechanical properties of polymer micro- and nano-composites containing fillers with a small aspect ratio of approximately one. Meanwhile, theoretical models that have been proposed to predict elastic modulus, strength and fracture toughness of particulate–polymer composites are also critically examined.

Polymer composites are noted to show mechanical properties which depend on time, rate and temperature [64]. Viscoelastic moduli are mainly governed by the volume fraction of particles [65] and strain rate has important effects on matrix/particulate interface adhesion and other mechanical properties [66–69]. Whilst this is a relevant topic, it is beyond the scope of this review and thus will not be discussed here. Interested readers may refer to the cited Refs. [64–69] and others in the published literature.

2. Young's modulus

Young's modulus is the stiffness (the ratio between stress and strain) of a material at the elastic stage of a tensile test. It is markedly improved by adding micro- and nano-particles to a polymer matrix since hard particles have much higher stiffness values than the matrix.

2.1. Experimental results

2.1.1. Effect of particle size

The effect of particle size (average diameter: 1, 2, 5, 8 and 12 μm) on the elastic modulus of epoxy/alumina trihydrate composites is shown in Table 1 [21]. It is seen that the modulus is not very much affected by particle size in the range studied.

The effects of particle loading and size (4.5–62 μm) on the elastic modulus of epoxy/spherical glass particle composites are given in Fig. 1 [22]. For lower volume fractions of glass beads (10–18 vol%), the modulus is almost independent of particle size. For higher glass bead loadings (30–46 vol%), there is a slight decrease in modulus with increasing particle size. These results imply that particle size has little effect on composite stiffness.

The effect of particle size on the modulus of an epoxy/silica composite has also been studied [70]. Spherical and irregular-shaped silica particles have different mean sizes in the range of 2–30 μm. Results show that the modulus remains constant with increasing particle size. Support is provided by test data obtained for a similar composite sys-

Table 1
Tensile modulus of the alumina trihydrate filled epoxy composites. Adapted from [21]

Particle size (μm)	Volume fraction (%)	Tensile modulus (GPa)
Unfilled	0	3.8
1	29.5	6.9
2	29.5	7.2
5	29.5	7.4
8	29.5	6.6
12	29.5	6.6

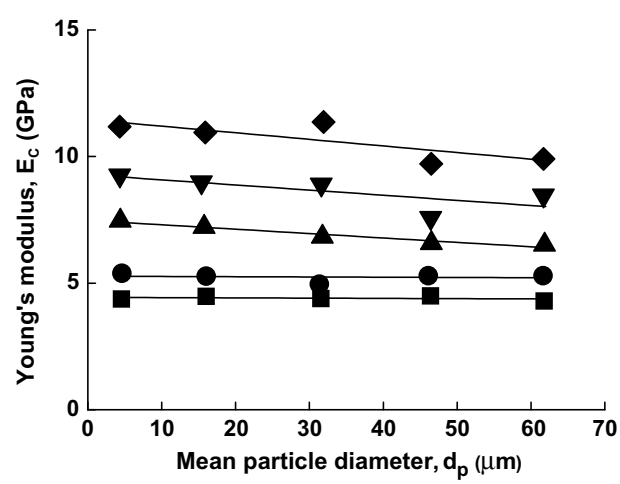

Fig. 1. Dependence of the modulus of glass bead filled epoxy composites with different volume fractions upon the particle size. The particle volume fraction is 10%, 18%, 30%, 40% and 46%, respectively from the bottom to top lines. Adapted from [22].

tem over a similar range of silica diameter 6–42 μm [15]. Note that the modulus of angular-shaped silica/epoxy composites decreases marginally with mean particle size (2–47 μm) [71]. The same observation is obtained for aluminum hydroxide filled polypropylene composites (where the average particle diameter varies from 1 to 25 μm) [72]. The elastic modulus of $CaCO_3$-filled polybenzoxazine composites increases with filler content but does not depend on particle size (1, 5 and 20 μm) [73]. Also, the modulus of aluminum particle/polyester composites is unaffected by particle size (100 nm, 3.5 and 20 μm) [74]. Similarly, particle size (1–12 μm) does not affect the modulus of epoxy/alumina trihydrate powder composites [75].

The tensile moduli of organo-soluble polyimide (PI)/silica composite materials are shown in Fig. 2 [16]. The silica particle size is dependent on its loading in the composite. Thus, it is 100–200 nm, 200–450 nm and 1–2 μm, respectively, for silica loading of 5, 10 and 20 wt%. Since Young's modulus increases linearly with silica content, the particle size effect is insignificant. Otherwise, the relationship will be non-linear [16].

In the above, it is shown that the particulate composite modulus is insensitive to particle size. However, when the particle is decreased to a critical size such as 30 nm, there will be an obvious effect of particle size on the modulus predicted theoretically as shown in Fig. 3 [76]. Indeed, it is also experimentally observed, Fig. 4 [77], that polypropylene (PP)/$CaCO_3$ composites containing smaller (21 nm) nanoparticles have higher Young's modulus than those composites with larger (39 nm) nanoparticles. Moreover, nanoindentation modulus has been obtained on composite coatings reinforced with silica of different sizes [78], as shown in Fig. 5. Clearly, the modulus decreases with increasing particle size from 15 to 35 nm, especially at high particle loading.

To summarize, it seems that there is a critical particle size above which there is no effect on composite modulus. When the particle size is below this critical value, the effect

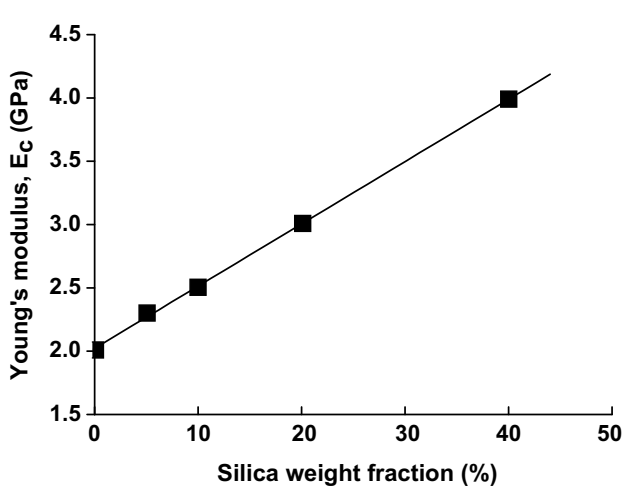

Fig. 2. The influence of silica content on the tensile modulus of polyimide/silica composite materials. Adapted from [16].

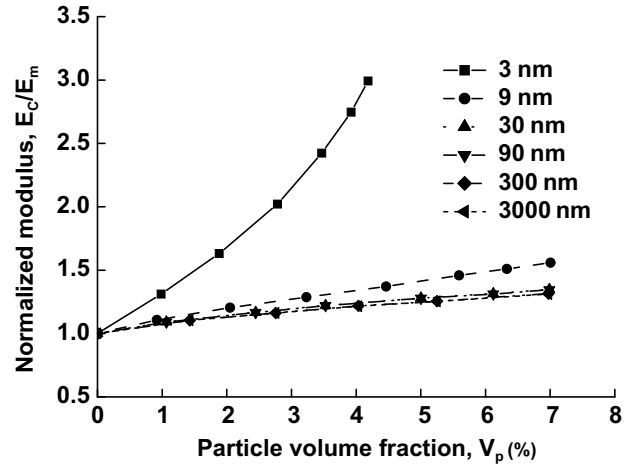

Fig. 3. The predicted modulus of spherical particle filled polymer composite as a function of particle size, where the particle to matrix modulus ratio $E_p/E_m = 40$. Adapted from [76].

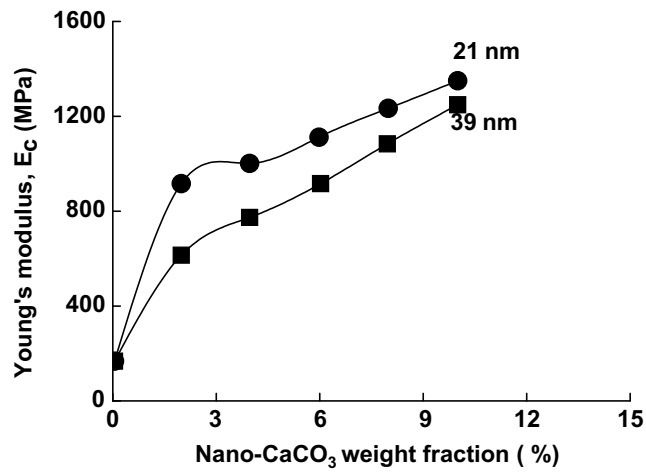

Fig. 4. Young's modulus of 21 nm and 39 nm $CaCO_3$ reinforced PP composites at different compositions. Adapted from [77].

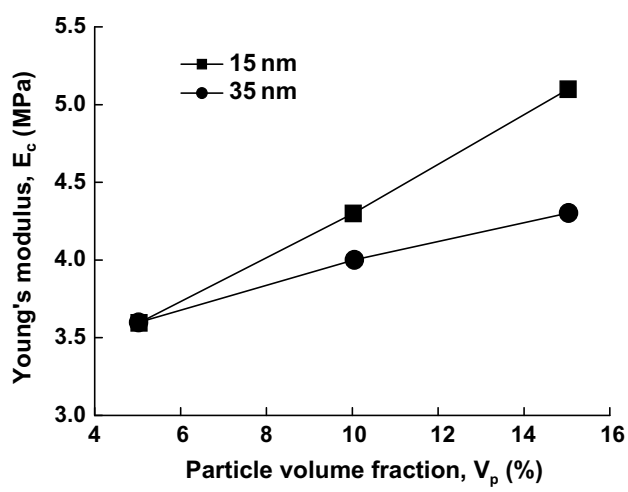

Fig. 5. The Young's modulus of polysiloxane nanocomposite coatings with different silica particle sizes as a function of the volume filler content. Adapted from [78].

on composite modulus is more significant. The magnitude of this critical particle size cannot be predicted *a priori* for it depends on the particle, matrix and particle/matrix adhesion.

2.1.2. Effect of particle/matrix interfacial adhesion

The tensile modulus of polystyrene (PS)/glass-bead composites is shown in Fig. 6 as a function of glass loading [17]. The bonding between glass and PS is varied by using different coupling agents. It is seen that the modulus is independent of the interfacial adhesion but increases almost linearly with glass loading. Since Young's modulus is measured at relatively low deformation, there is insufficient dilation to cause interface separation. Thus, it is easy to understand that the adhesion strength does not noticeably affect the elastic modulus.

Many studies have supported the above observation. Young's modulus of epoxy/glass bead composites increases with glass bead loading [79] but is unaffected by glass surface treatment. Moreover, the effect of interfacial bonding on flexural modulus of glass bead ($d_p \sim 30$ μm) filled epoxy and polyester resins is studied as a function of particle volume fraction and interfacial bond strength [62]. The latter parameter can be varied by chemical surface treatment of glass using a silicone mold release to prevent chemical bonding at one extreme and a silane coupling agent to maximize bonding at the other extreme. No clear effect of interfacial bonding on modulus can be seen. Similar results are also obtained on the modulus of nanocomposites. For example, the modulus of a polypropylene composite filled with 0–40 vol% of ultra-fine calcium carbonate ($d_p =$ 70 nm) is studied [35]. Untreated and surface treated particles are considered. A monotonic increase in modulus is noted with filler loading but no noticeable effect of interfacial adhesion on modulus has been found.

Conversely, it is observed that the modulus of polypropylene (PP)/$BaSO_4$ composites depends on interfacial modification but this is an indirect effect [80]. It is shown from

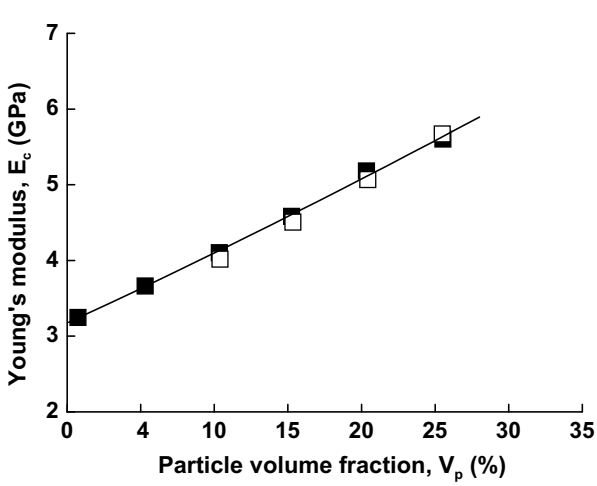

Fig. 6. The Young's modulus at 20°C for PS–glass bead composites with excellent (□) and poor (■) interfacial adhesion. Adapted from [17].

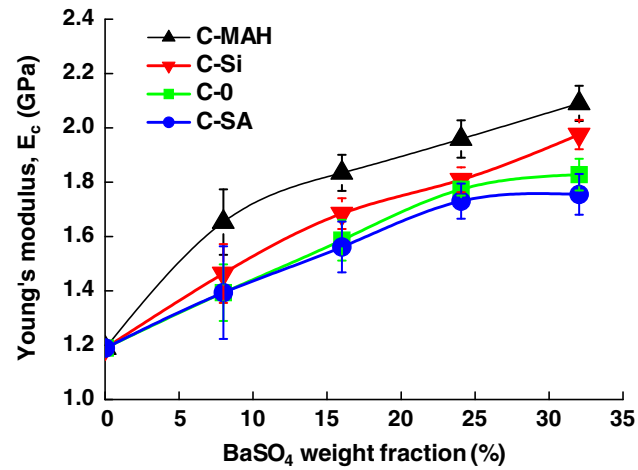

Fig. 7. The Young's modulus of the PP/$BaSO_4$ composites. M-0: virgin PP + $BaSO_4$ without pretreatment; M-SA: virgin PP + $BaSO_4$ pretreated with 1 wt% stearic acid; M-SI: virgin PP + $BaSO_4$ pretreated with 1 wt% silane AMPTES; M-MAH: PP-g-MAH + $BaSO_4$ without pretreatment. The resultant composites were designated hereafter as C-0 for PP/M-0, C-SA for PP/M-SA, C-SI for PP/M-SI and C-MAH for PP/M-MAH, respectively. Adapted from [80].

Fig. 7 that the composite modulus is controlled to some extent by particle surface modification. This phenomenon is due to two possible factors: interfacial adhesion and matrix crystalline structure. The direct effect of the former is insignificant since modulus is a property at low deformation which is not sensitive to adhesion. The second factor is mainly responsible for the improvement of composite modulus because the crystallinity of semi-crystalline polymers, and hence the composite modulus [80], is affected by the filler.

In conclusion, interfacial adhesion has little effect on the Young's modulus of particulate-filled composites.

2.1.3. Effect of particle loading

The effect of particle loading on composite modulus has actually been already shown in Figs. 1–7 for some material systems, in which the modulus increases with increasing particle loading. More examples are given below to demonstrate this effect.

Table 2 lists Young's modulus of hydroxyapatite (HA) filled polymer composites [24]. It is clear that modulus is strongly dependent on particle loading. When 10 vol% particles are added, the modulus is increased by ~50–100%. Similar results for other particulate–polymer composite systems have also been obtained. For example, it is observed that the tensile modulus of ternary polymer composites: polyamide 6,6 (PA 6,6)/poly[styrene-*b*-(ethylene-*co*-butylene)-*b*-styrene] grafted by maleic anhydride (SEBS-g-MA)/glass beads, is enhanced by adding glass beads (with an average size ~32 μm) [33]. Also, the modulus of epoxy/glass bead composites increases with glass bead volume fraction [23]. Similarly, the elastic modulus of nylon 6/silica nanocomposites increases constantly with

Table 2
Young's modulus of hydroxyapatite (HA) particle filled polymer composites. Adapted from [24]

HA volume fraction (%)	Young's modulus (GPa)			
	HA P88/HDPE[a]	HA P81B/HDPE[a]	HA P88/XPE[a]	HA P81B/XPE
0	0.65 ± 0.02	0.72 ± 0.03	1.37 ± 0.07	1.37 ± 0.07
10	0.98 ± 0.02	0.98 ± 0.07	2.04 ± 0.11	2.07 ± 0.03
20	1.60 ± 0.02	1.55 ± 0.04	2.77 ± 0.14	3.05 ± 0.09
30	2.73 ± 0.10	2.46 ± 0.21	4.38 ± 0.18	4.48 ± 0.17
40	4.29 ± 0.17	3.74 ± 0.14	5.97 ± 0.25	6.48 ± 0.17
45	5.54 ± 0.62	5.39 ± 0.81	7.63 ± 0.42	6.95 ± 0.40

[a] Note: HA P88 and HA P81B have, respectively, average particle size of 4.14 and 7.32 μm. HDPE: high density polyethylene and XPE: cross-linkable polyethylene.

increasing silica loading as shown in Fig. 8 [30], where the particle size varies from 50 to 110 nm.

Hence, addition of rigid particles to a polymer matrix can easily improve the modulus since the rigidity of inorganic fillers is generally much higher than that of organic polymers. The composite modulus consistently increases with increasing particle loading.

2.2. Theories for elastic modulus

The elastic modulus of a particulate–polymer composite is generally determined by the elastic properties of its components (particle and matrix), particle loading and aspect ratio [19,81–83]. When the aspect ratio of particles equals unity, such as for spherical particles, the composite modulus will then depend on the modulus of the components and particle loading or particle size as described in Section 2.1. Since the modulus of inorganic particles is usually much higher than that of the polymer matrices, the composite modulus is easily enhanced by adding particles to matrix. Many empirical or semi-empirical equations have been proposed to predict the modulus of particulate–polymer composites and these are summarized below.

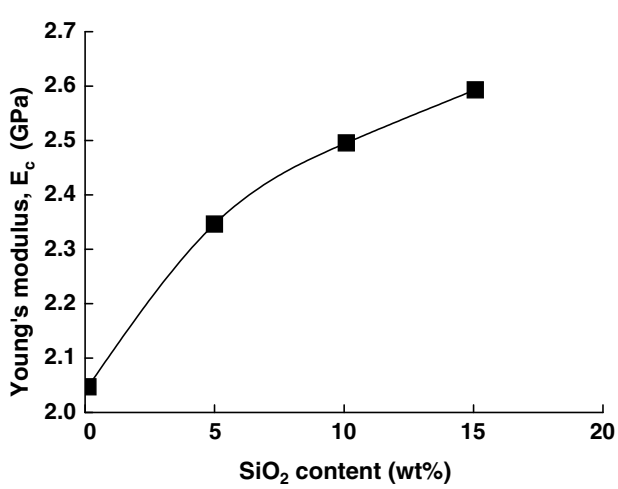

Fig. 8. Tensile modulus of nylon 6 nanocomposites as a function of SiO_2 particle content. Adapted from [30].

Based on the rigid particle assumption, Einstein's equation for prediction of the Young's modulus of particulate composites is [84,85]

$$E_c/E_m = 1 + 2.5V_p \tag{1}$$

where E_c and E_m are Young's modulus of composite and matrix, and V_p is particle volume fraction. Einstein's equation was originally derived for the effective shear viscosity for dilute suspensions of rigid spheres and was extended to study the effective viscosity of concentrated suspensions of mono-sized spheres [86]. The above simple Einstein equation (1) for Young's modulus of particulate composites is valid only at low concentrations of filler and assumes perfect adhesion between filler and matrix, and perfect dispersion of individual filler particles [87]. This equation implies that the composite modulus is independent of particle size and predicts a linear relationship between E_c and V_p. It is useful for low particle loading but not suitable for large loading due to the interaction of the strain fields around the particles. Hence, there are several modifications to Einstein's equation. Guth [88] added a particle interaction term in the Einstein equation which becomes

$$E_c/E_m = 1 + 2.5V_p + 14.1V_p^2 \tag{2}$$

where the linear term is the stiffening effect of individual particles and the second power term is the contribution of particle interaction.

Halpin and Tsai found that the modulus of particulate polymers can be predicted by the semi-empirical relationship [89,90]

$$E_c/E_m = \frac{1 + A_1B_1V_p}{1 - B_1V_p} \tag{3}$$

where A_1 and B_1 are constants for a given composite. A_1 is a function of the particle shape and matrix Poisson ratio, and B_1 is related to the modulus of the particle (E_p) and matrix (E_m). Another elaborate equation for estimating the modulus of a composite that contains spherical particles in a matrix is due to Kerner [91] and given below

$$E_c/E_m = 1 + \frac{V_p}{(1 - V_p)}\frac{15(1 - \nu_m)}{(8 - 10\nu_m)} \tag{4}$$

for $E_p \gg E_m$ and v_m is the matrix Poisson ratio. Based on Eqs. (3) and (4), Nielsen [92–94] suggested the following more general equation:

$$E_c/E_m = \frac{1 + A_1 B_1 V_p}{1 - \Psi B_1 V_p} \tag{5a}$$

where Ψ depends on particle packing fraction and constants A_1 and B_1 are defined below. Thus, we have

$$A_1 = k_E - 1, \quad B_1 = \frac{E_p/E_m - 1}{E_p/E_m + A} \tag{5b – d}$$

$$\Psi = 1 + [(1 - V_{p\,max})/V_{p\,max}^2]V_p$$

where k_E is Einstein's coefficient and $V_{p\,max}$ is maximum packing fraction.

Mooney [95] made another modification to the Einstein equation as follows:

$$E_c/E_m = \exp\left(\frac{2.5V_p}{1 - sV_p}\right) \tag{6}$$

where s is a crowding factor for the ratio of the apparent volume occupied by the particle to its own true volume, and its value lies between 1.0 and 2.0. This modified equation is reduced to Einstein's equation (1) at low volume fractions of spherical particles and represents test data at high volume fractions. For non-spherical particles, Mooney's equation is further modified to [96]

$$E_c/E_m = \exp\left(\frac{2.5V_p + 0.407(P-1)^{1.508}V_p}{1 - sV_p}\right) \tag{7}$$

where P is the aspect ratio of the particle with $1 \leqslant P \leqslant 15$.

The simplest arrangements of fibres in a two-phase material containing continuous fibres and matrix are series (Reuss) and parallel (Voigt), and assuming iso-stress and iso-strain criteria for these two cases, respectively, a lower-bound of the composite modulus

$$E_c^{lower} = E_p E_m/[E_p(1 - V_p) + E_m V_p] \tag{8}$$

and an upper-bound

$$E_c^{upper} = E_p V_p + E_m(1 - V_p) \tag{9}$$

can be derived. Voigt's model gives a linear relationship between E_c and V_p and a gross over estimate of E_c. The modulus of real composites lies between these two bounds. These upper- and lower-bound models are applicable to most particulate micro- and nano-composites. Generally, the modulus of composites should be lower than the upper-bound predicted by Eq. (9) and higher than the lower-bound by Eq. (8) [97], although it is possible for a composite to violate the Voigt–Reuss bounds due to Poisson's effect [98]. An example is shown in Fig. 9 for silica filled PA 6 nanocomposites [29], where the particle size varies in a narrow range of 12, 25 and 50 nm. The experimental data lie between these two bounds. And Kerner's equation (4) gives much better agreement with the test results, where the matrix Poisson ratio was assumed to be 0.3 [29]. Based on the series and parallel models, Coran [99] suggested the following equation to estimate the effective Young's modulus:

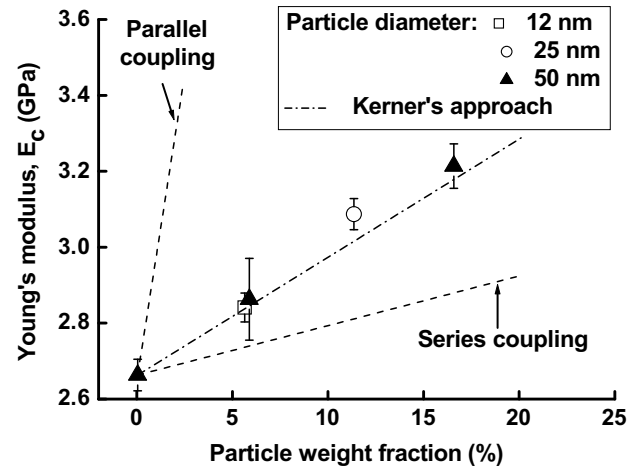

Fig. 9. Variation of the tensile modulus of silica-filled PA6 nanocomposites with respect to the filler content for various mean particle sizes: 12, 25 and 50 nm. Adapted from [29].

$$E_c = f_c(E_c^{upper} - E_c^{lower}) + E_c^{lower} \tag{10}$$

where f_c is a factor of the phase morphology and can vary between 0 and 1. Coran's equation has been adopted by George et al. [100,101] with good effect.

In addition, Hashin and Shtrikman [102] and others (see [103] and references therein) have developed sharper bounds (namely in a narrower range between the two bounds) for elastic moduli of composites. This type of methods can only give two bounds but cannot predict the exact value of the composite modulus.

Counto [104] proposed a simple model for a two-phase particulate composite by assuming perfect bonding between filler and matrix. The composite modulus is given by

$$\frac{1}{E_c} = \frac{1 - V_p^{1/2}}{E_m} + \frac{1}{(1 - V_p^{1/2})/V_p^{1/2}E_m + E_p} \tag{11}$$

This model predicts moduli in good agreement with a wide range of test data.

Ishai and Cohen [105] and Paul [106] assumed that the two constituents are in a state of macroscopically homogeneous stress and adhesion is perfect at the interface of a cubic inclusion in a cubic matrix. When a uniform stress is applied on the boundary, the elastic modulus of the particulate composite is given by

$$E_c/E_m = 1 + \frac{1 + (\delta - 1)V_p^{2/3}}{1 + (\delta - 1)(V_p^{2/3} - V_p)} \tag{12}$$

which is another upper-bound solution. Using the same model, with uniform strain applied at the boundary, Ishai and Cohen [105] obtained a lower-bound solution

$$E_c/E_m = 1 + \frac{V_p}{\delta/(\delta - 1) - V_p^{1/3}} \tag{13}$$

where $\delta = E_p/E_m$. The dependence of Young's modulus of epoxy/glass bead composites and epoxy/rubber has been tested by using the model, that is, Eqs. (12) and (13) [107]. However, only the lower-bound solution fits the data well. This observation has also been found by Young et al. [108]. Nonetheless, the model should give upper- and lower-bounds to the composite modulus [109], namely, all data lie between the two bounds described by Eqs. (12) and (13). Indeed, the modulus results obtained for PP/ultra-fine $CaCO_3$ composites fell within these two bounds.

For simplicity and without loss of accuracy, an approximate method, that is, the modified rule of mixtures, can also be used to predict the elastic modulus of particulate composites [110]

$$E_c = \chi_p E_p V_p + E_m(1 - V_p) \tag{14}$$

where $0 < \chi_p < 1$ is a particle strengthening factor. The elastic moduli of particulate composites predicted by Eq. (14), originally developed for modulus of short-fibre composites [18,111–113], fall between those predicted by the Reuss (Eq. (8)) and Voigt models (Eq. (9)).

Verbeek [114] provided another model for evaluating the composite modulus by the following equation:

$$E_c = \chi_p E_p V_p + E_m(1 - V_p) \tag{15}$$

where $\chi_p = 1 - \tanh(V_{p\,max})/V_{p\,max}$. The model assumes perfect adhesion between the phases and that stress is transferred via a shear mechanism. Good agreement is obtained for the moduli of low density polyethylene (LDPE)/phlogopite composites at different particle sizes as shown in Fig. 10. The two sets of data correspond to both narrow and wide size distributions. It does not seem that particle size has any significant effect on the modulus.

The modulus of silica filled ethylene–vinyl acetate copolymer is found to be very sensitive to particle size, e.g. changing the size from 600 nm to 14 nm increases the modulus several-fold [115]. Indeed, the elastic moduli of several polymer/inorganic nanocomposites are so high that two-phase models cannot describe the test results [116–120]. Takayanagi et al. noticed the formation of micro-fibrils with diameters 10–30 nm and these micro-fibrils were more influential at interphase boundaries than in bulk [121]. Thus, an interphase region was added to formulate the tensile modulus of such polymer nanocomposites and the effect of nanosized spherical particles could thus be accommodated [76]. From the predicted results, there is a critical particle size of ~30 nm below which composite modulus increases with decreasing particle size. Supporting experimental evidence has come from Mishra et al. [77] and Douce et al. [78].

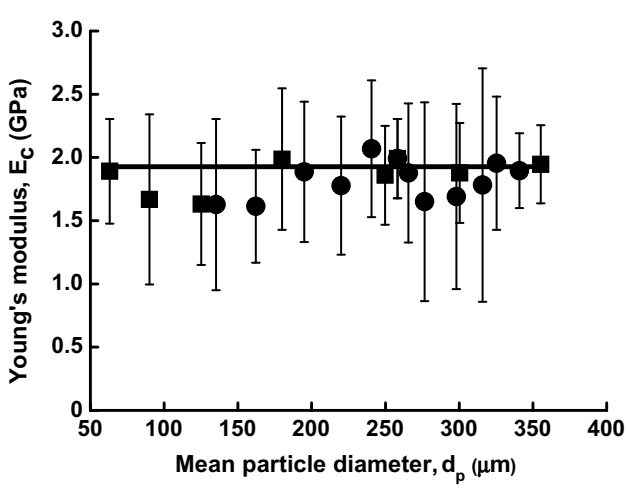

Fig. 10. Variation of Young's modulus with particle size and size distribution of phlogopite, at constant aspect ratio for narrow (■) and wide (●) distributions. The predicted values from Eq. (15) are shown as the solid line. Adapted from [114].

Besides the abovementioned empirical or semi-empirical formulas and the bounding techniques micromechanics has already made a great success in prediction of the overall effective elastic moduli of composites [103,122]. Micromechanics approaches deal with the weak and strong dependences of material properties on particle interaction. Various micro-mechanics schemes have been established to estimate the effective moduli, which depend mainly on the statistically averaged effect of particle interaction. The simplest one is the non-interacting method (also referred to as Taylor's model or dilute concentration model, DCM), which neglects completely the interaction of particles. It may offer quite accurate results in most cases of low volume fractions of the reinforcing phase. When considering statistical effects of inclusions, the effective moduli may be estimated using the self-consistent method, Mori–Tanaka method [123], differential method, generalized self-consistent method and other approaches based on the concept of effective medium or effective field. These conventional techniques, with few exceptions, neglect the precise locations and orientations of particles. Therefore, their applications are limited to solids that are statistically homogeneous and subjected to uniform tractions or displacements on their surfaces. In addition, the statistical micromechanical theory, stochastic defect theory, and some other micromechanical theories [103] may be considered to elucidate the effects of particulate interaction. However, due to cumbersome calculations, they are difficult to be implemented in a framework of effective moduli of materials with profuse particles.

In micromechanics methods, the key problem in estimation of effective moduli of composites is how to calculate the average strain of an Eshelby inclusion embedded in a solid containing many dispersed inclusions. Evidently, it is difficult to determine the exact solution due to the large number of interacting particles whose orientations and locations are often distributed statistically. Therefore, some simplifications or approximations are necessary. On one hand, the medium surrounding an inclusion is disturbed by the complex microstructure, and then has a stiffness different from the pristine matrix. Conversely, the stress field around an inclusion is perturbed due to the existence of other particles. Thus, as a straightforward approximate

model, the inclusion is assumed to be surrounded by an effective medium, also referred to as the reference matrix, with a stiffness (or compliance) and subjected to an effective stress (or strain) in the far field. This approximation, which renders the analytical evaluation of the effective moduli of a heterogeneous solid, is common to all the effective medium methods and the effective field methods aforementioned, although the definitions of the effective medium and the effective field in these methods are different.

A rather simple and accurate micromechanics method is Mori–Tanaka method [123]. It assumes each inclusion in the infinite pristine matrix loaded by an effective stress that equals the average stress over the matrix. The effective moduli of inclusion-dispersed composites may be easily derived with good accuracy even for a high volume fraction of inclusions. For a composite reinforced by particles of spherical shape, this method leads to the effective Young's modulus E_c, bulk modulus $\widetilde{K}_m$ and shear modulus $\widetilde{G}_c$ as

$$E_c = \frac{9\widetilde{K}_c\widetilde{G}_c}{3\widetilde{K}_c + \widetilde{G}_c} \tag{16a}$$

$$\widetilde{K}_c = \widetilde{K}_m + \frac{V_p\widetilde{K}_m(\widetilde{K}_p - \widetilde{K}_m)}{\widetilde{K}_m + \beta_2(1 - V_p)(\widetilde{K}_p - \widetilde{K}_m)} \tag{16b}$$

$$\widetilde{G}_c = \widetilde{G}_m + \frac{V_p\widetilde{G}_m(\widetilde{G}_p - \widetilde{G}_m)}{\widetilde{G}_m + \beta_1(1 - V_p)(\widetilde{G}_p - \widetilde{G}_m)} \tag{16c}$$

where $\beta_1 = \frac{2(4-5\nu_m)}{15(1-\nu_m)}$, $\beta_2 = 3 - 5\beta_1$, $\widetilde{K}$ and $\widetilde{G}$ denote the bulk modulus and the shear modulus, the subscripts "m" and "p" stand for matrix and particulate, respectively. Many other analytical or semi-analytical solutions from micromechanics methods are available in the literature but are omitted here for conciseness.

The effect of particle size on the effective elastic modulus of composites has recently attracted much attention, especially for nanoparticle-reinforced composites. The particles restrict the mobility and deformation of the matrix by introducing a mechanical restraint. The restriction in polymeric molecular diffusion in the presence of solid particles occurs because of an effective attraction potential between segments of the chain and the repulsive potential that the polymer is subjected to when it is close to solid particles. The degree of the particle restriction depends on the properties of the filler and the matrix [124,125]. This effect of interfacial phase or interphase also makes a contribution to the enhancement in the composite modulus. For particles of size larger than 1 μm, however, this contribution will be negligible compared to that of the particles. The zero-thickness assumption for interfaces is generally acceptable. The reasons are twofold. First, the restriction to the mobility and deformation of matrix by particles should be limited to a very small volume for a low V_p because the thickness of interphase is generally about 1 nm or smaller and the content of particles added in composites is usually small. Second, while for a high V_p the elastic modulus of the confined polymer near interfaces is much lower than that of the particles, though higher than the unconfined polymer. This independence of elastic modulus of particle-filled micro-composites is consistent with the prediction of conventional micromechanics which neither has an internal length parameter in its constitutive relation nor accounts for the interphase effects. In addition, Christensen and Lo's three-phase model [126], Mori–Tanaka method, self-consistent method, Halpin and Kardos' model [127] of micromechanics can also be extended to account for the interface effect by including an interphase region between the matrix and particles [128,129]. For instance, Colombini et al. [130,131] used the self-consistent scheme based on a "particle-interphase-matrix" three-phase unit cell model to study the influence of the particle size and shape on the mechanical properties of bimodal hard/soft latex blends. They found that the smaller the size of the hard particles, the better the mechanical enhancement of the mechanical film properties. Sevostianova and Kachanov [132] used a differential scheme suggested by Shen and Li [133] to account for the interphase effect on effective elastic moduli. Lutz and Zimmerman [134] addressed the effect of an inhomogeneous interphase zone on the bulk modulus and conductivity of particulate composites.

For reviews and recapitulations of micromechanics theories and the related results, the reader is referred to Refs. [103,122] and references cited therein. Most previous work was conducted based on Eshelby's inclusion theory [135] for those composites comprised of well-defined inclusions dispersed in a connected matrix phase. The conventional Eshelby's tensor was derived for elliptical inclusions perfectly bonded to the matrix by assuming that the interface region has a zero thickness. To account for the size effect of particles, the classical formulation of Eshelby's theory has been revisited to include the surface/interface stresses, tension and energy [136]. The influences of such factors as particle agglomeration and interface debonding on the elastic moduli have also been studied recently (see for example, [137–141] and references therein).

3. Strength

The strength of a material is defined as the maximum stress that the material can sustain under uniaxial tensile loading. For micro- and nano-particulate composites this relies on the effectiveness of stress transfer between matrix and fillers. Factors like particle size, particle/matrix interfacial strength and particle loading that significantly affect the composite strength are discussed below.

3.1. Experimental results

3.1.1. Effect of particle size

The effect of spherical particle size on the tensile yield strength of polypropylene (PP)/$CaCO_3$ composites is shown in Fig. 11 [27]. The particle size varies from 10 nm, 80 nm, 1.3 to 58 μm. It is clearly shown that, for a given particulate volume fraction, the composite strength increases with decreasing particle size. Smaller particles

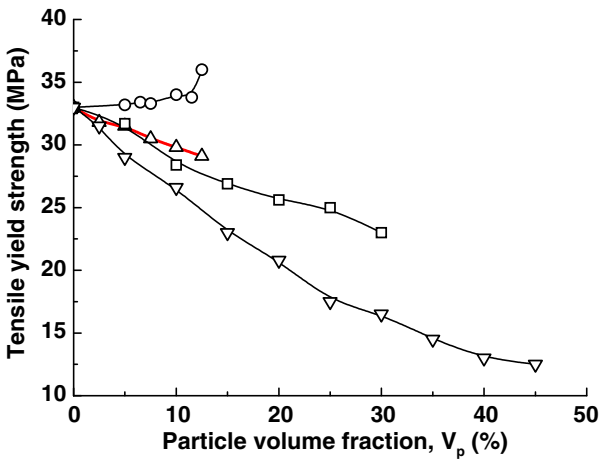

Fig. 11. Effect of spherical filler particle size on tensile yield strength of PP–$CaCO_3$ composites. Particle diameter: (○) 0.01 μm, (△) 0.08 μm, (□) 1.3 μm and (▽) 58 μm. Adapted from [27].

have a higher total surface area for a given particle loading. This indicates that the strength increases with increasing surface area of the filled particles through a more efficient stress transfer mechanism. However, it is noted that for particles at and larger than 80 nm, the composite strength is reduced with increasing particle loading. For the 10 nm-particle composites the trend is reversed. If nanocomposites are defined as having particles with at least one dimension smaller than 100 nm [6], then the strength results in Fig. 11 suggest that nanocomposites with $CaCO_3$ nanoparticles may show a decrease in strength as the particle loading increases.

The effect of particle size on composite strength of PA 6/silica nanocomposites is shown in Fig. 12 [29], where the mean sizes are 12, 25 and 50 nm, respectively. Addition of particles leads to an increase in strength; and smaller particles give better reinforcement. These results are in agreement with those obtained by Sumita et al. [58] over the same range of filler size. In a similar study of mechanical properties of kaolin filled nylon 6,6 composites [142], it is found that the composite strength also increases with decreasing mean particle size (0.4–4.8 μm).

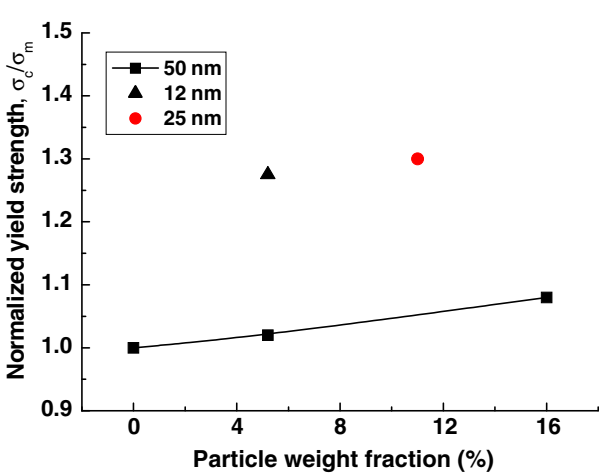

Fig. 12. Variation of the tensile yield strength of silica-filled PA6 nanocomposites with respect to the filler content for various mean particle sizes: 12, 25 and 50 nm. Adapted from [29].

Fig. 13 presents the tensile strength results of epoxy/silica composites as affected by the mean silica particle size within the micro-scale range [28]. There is a large improvement in tensile strength with decreasing particle size. This trend is supported by the tensile strength results of epoxy/alumina trihydrate particulate composites in Table 3 [21] and other composites [70,71,143] such as $Mg(OH)_2$/ethylene–propylene–diene terpolymer (EPDM) [71] in Fig. 14. It is shown that, at the same particle loading, nano-$Mg(OH)_2$ is more efficient than micro-$Mg(OH)_2$ to strengthen epoxy matrix.

To conclude, particle size clearly has a significant effect on the strength of particulate-filled polymer composites, which generally increases with decreasing size.

3.1.2. Effect of particle/matrix interfacial adhesion

As in fibre-reinforced composites, the quality of adhesion at the interface is of crucial importance for the behaviour of particulate composites. The adhesion strength at the interface determines the load transfer between the components. The Young's modulus, however, is not affected by this parameter because, for small loads or displacements,

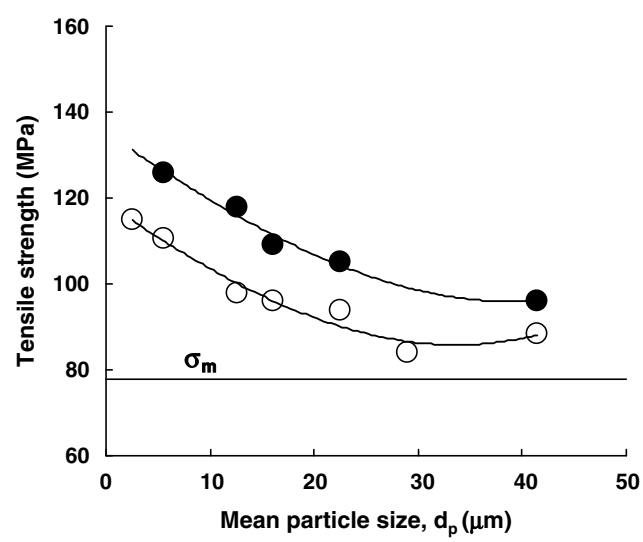

Fig. 13. Effect of particle size on tensile strength of epoxy composites filled with spherical silica particles with particle contents of 55 wt% (○) and 64 wt% (●). The dotted line represents the matrix strength σ_m. Adapted from [28].

Table 3
Tensile strength of alumina trihydrate filled epoxy composites. Adapted from [21]

Particle size (μm)	Volume fraction (%)	Tensile strength (MPa)
Unfilled	0	75.9 ± 8.8
1	10	58.0 ± 3.4
8	10	29.9 ± 1.7
12	10	27.2 ± 2.4

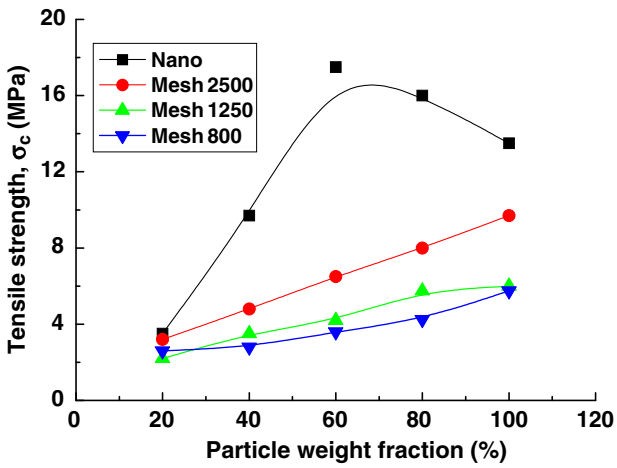

Fig. 14. Effect of $Mg(OH)_2$ loading with different particle sizes on tensile strength of $Mg(OH)_2$/EPDM composites. [In the inset: nano, 2500 mesh, 1250 mesh and 800 mesh mean 50/100 nm, 2.03 μm, 2.47 μm and 2.93 μm, respectively.] Adapted from [71].

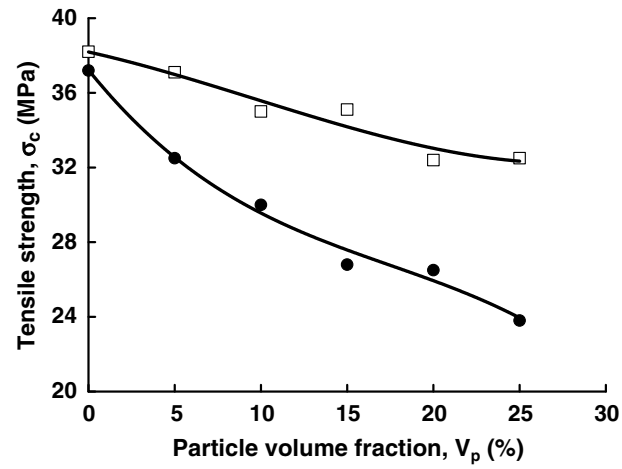

Fig. 15. The tensile strength at 20 °C for PS–glass bead composites with excellent (□) and poor (●) interfacial adhesion. Adapted from [17].

debonding is not yet observed. On the other hand, composite strength and toughness are very much dependent on the adhesion quality.

To evaluate adhesion between two different materials there are different approaches. The work of adhesion can be determined by contact angle measurement or by contact mechanics, a critical discussion is given by Packham [144]. To understand the basic mechanisms at a polymer surface, which are responsible for adhesion at the molecular level, the reader, is referred to the survey given by Creton et al. [145]. Another method was direct determination of the adhesion strength between a single particle and the surrounding matrix. Harding and Berg [146] used a cylindrical specimen with an embedded single particle, whereas Mower and Argon [147] and Lauke [148] used curved specimens. The tests provide the adhesion strength at the interface between particle and matrix and between particle and interphase, respectively.

In Fig. 11, the strength of micro-particle-filled composites decreases with particle content. In Figs. 13 and 14, the reverse is true, i.e. in micro-size, strength increases with particle content. This contradiction is because, besides particle size and loading, the particle/matrix interfacial adhesion also significantly affects the strength of particulate composites, and this is discussed below. Effective stress transfer is the most important factor which contributes to the strength of two-phase composite materials. For poorly bonded particles, the stress transfer at the particle/polymer interface is inefficient. Discontinuity in the form of debonding exists because of non-adherence of particle to polymer. Thus, the particle cannot carry any load and the composite strength decreases with increasing particle loading. However, for composites containing well-bonded particles, addition of particles to a polymer will lead to an increase in strength especially for nanoparticles with high surface areas.

The tensile strengths of polystyrene (PS)/glass bead composites are shown in Fig. 15 [17]. The glass beads have a diameter ~10–53 μm. The interface bonding strength between glass and polystyrene is varied by using different coupling agents. The composite strength decreases with increasing glass content and is lower than that of the polymer matrix; but better interfacial adhesion gives higher composite strength. During tensile testing, crazes form at a critical applied stress. In poorly bonded beads, de-wetting along the phase boundary [149] introduces a small cap-shaped cavity at the top of the bead. This cavity will induce extra stress concentration in the vicinity of its relatively sharp edge. Thus, craze formation at the edge of the cavity occurs at a lower applied stress when compared to the case of well-bonded beads, in which de-wetting is absent as the crazes directly form near the poles of the bead.

In nylon 6-based nanocomposites, an obvious effect of particle/matrix interface adhesion on composite strength

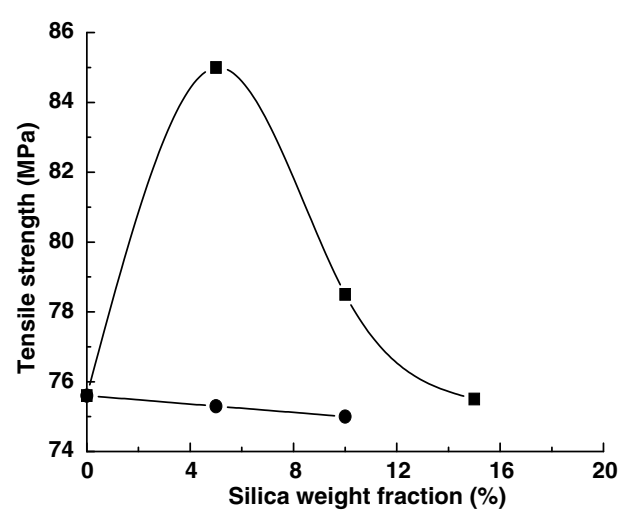

Fig. 16. Tensile strength of nylon 6 nanocomposites filled with modified (■) and unmodified (●) silica (SiO_2) particles, respectively. Adapted from [30].

also exists [30]. If the particles, whose size varies from 50 to 110 nm, are untreated, the strength decreases only marginally with increasing particle content. However, when the surface of silica nanoparticles is modified by aminobutyric acid to improve the filler/matrix adhesion, the tensile strength of nylon 6/silica nanocomposites shows a bell-shaped curve with silica loading (Fig. 16). The modified composites have good particle dispersion and strong polymer/silica interface adhesion for effective stress transfer. Therefore, the composite strength is increased. When silica content is above 5 wt% particle aggregation occurs, thus leading to degradation in composite strength as the particle content increases.

The incorporation of a small amount of $BaSO_4$ particles in polypropylene (PP) does not significantly affect the yield strength of the composites (Fig. 17) [80], whereas a relatively high content of $BaSO_4$ particles (>16 wt%) has a negative effect on the yield strength. It is noted that the yield strength depends on the interfacial modification. C-MAH (PP/M-MAH) and C-SI (PP/M-SI), with interfaces modified with PP-g-MAH and silane, have higher yield strength than that without modification (C-0) or modified with stearic acid (C-SA), showing pronounced reinforcements.

Zhang and co-workers [141,150] studied the effect of interfacial adhesion on the strength of PP/silica nanocomposites, in which nanosilica particles were treated by various monomers (e.g., styrene, methyl and methacrylate) to obtain different interfacial interactions. Thio et al. [151] also examined the influence of interfacial adhesion on the mechanical properties of PP/glass composites. The glass particles were treated with two silanes having different functional groups, hydrocarbons and fluorocarbons. These investigations found that the tensile strengths of the reinforced polypropylenes increased with increasing interface adhesion. The tensile strengths of nylon 6,6/kaolin composites, whereby the particles were treated with an amino-silane coupling agent, were determined [142]. It is also shown that the composite strength is increased when the interface adhesion is improved.

From the above discussions, it is apparent that the particle/matrix interfacial adhesion has a prominent effect on the strength of particulate-filled polymer micro- and nano-composites. A strong interfacial bonding between particles and polymer matrix is critical for effective stress transfer leading to high composite strength. Vice-versa, a weak particle/matrix interface bonding will only give low composite strength.

3.1.3. Effect of particle loading

The effects of particle size and particle/matrix interface adhesion on the strength of particle reinforced micro- and nano-composites are discussed above. For some systems, the effect of particle loading on strength is also shown. To cover a wider range of materials, however, more details are given below for other micro- and nano-composites.

The tensile strength of organo-soluble polyimide (PI)/silica hybrid films is shown in Fig. 18 [16]. The silica particle size in the hybrid (composite) is 100–200 nm for the silica content of 5 wt%. When the silica content is increased to 10 and 20 wt%, the particle size is increased to 200–450 nm and 1–2 μm, respectively. The strength increases with silica content up to ~10 wt% at which time the tensile strength is improved by ~33%. For larger silica content, the particles are micron-sized and the composite strength decreases. For ultra-fine calcium carbonate particle-filled polypropylene composites (particle diameter is 70 nm), the strength has been studied in the composition range 0–40 vol% [35]. Untreated and surface-treated fillers are used. The results show monotonic decrease in strength with particle volume fraction for both fillers. Recently, Kuo et al. [107] fabricated poly(ether–ether–ketone) (PEEK) polymer composites reinforced with nanosized (15–30 nm) silica or alumina particles (5–7.5 wt%) by vacuum hot pressing. The optimal increase in tensile strength is ~20–50%. Jiang

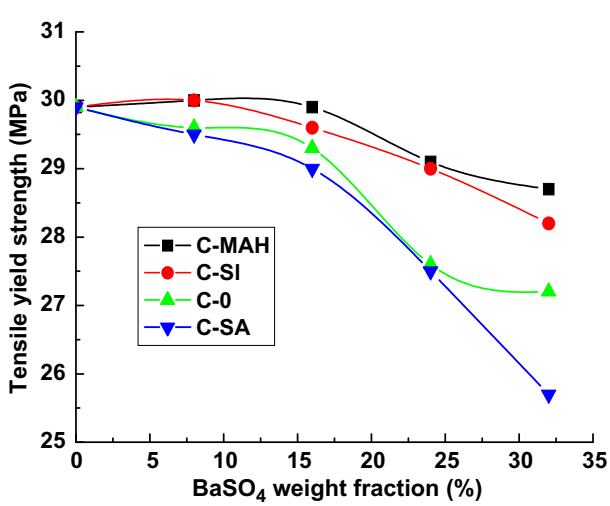

Fig. 17. The yield stress of the neat PP and the PP/$BaSO_4$ composites. Adapted from [80].

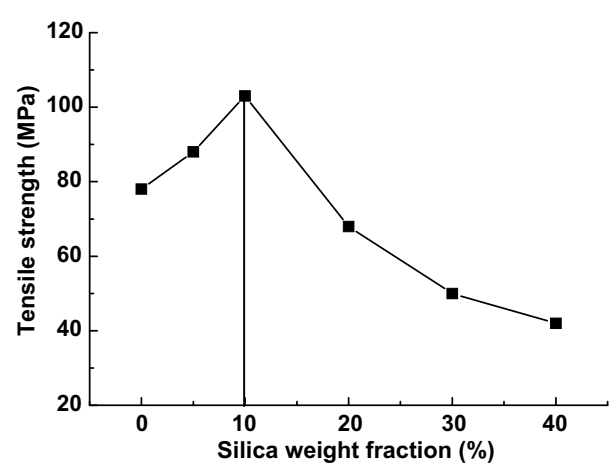

Fig. 18. Influence of silica content on the tensile strength of polyimid/silica composite films. Adapted from [16].

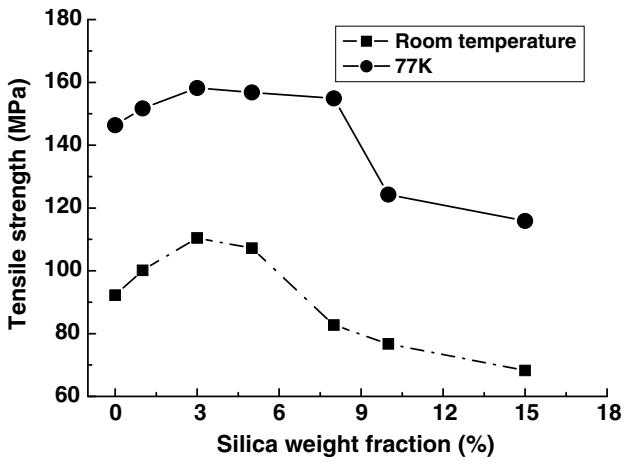

Fig. 19. The tensile strength of SiO_2/PI hybrid films at room temperature and 77 K as a function of silica content. Adapted from [153].

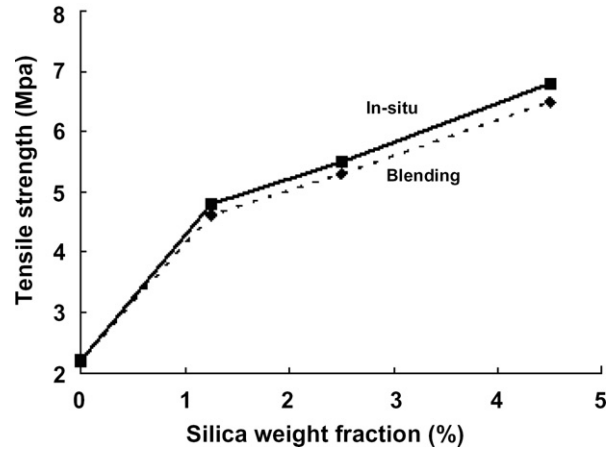

Fig. 20. Tensile strength of polyurethane/nanosilica composites prepared via *in situ* polymerization and blending methods as a function of silica concentration (silica particle size 66 nm). Adapted from [156].

et al. recently reported fabrication of semi-crystalline polylactide (PLA) nanocomposites with nanosized precipitated calcium carbonate (NPCC) by melt extrusion [152]. However, the addition of NPCC in the range ~2.5–7.5 wt% results in a reduction of tensile strength of the resulting nanocomposites.

Fig. 19 displays the tensile strength of polyimide (PI)/SiO_2 hybrid films prepared using *in situ* sol–gel process as a function of silica content [153]. The tensile strength at both room (298 K) and liquid nitrogen (77 K) temperatures increases first to a maximum, and afterwards decreases with increasing silica content [153]. These results are caused by the fact that silica particle size is in nm when its content is below 8 wt% and, beyond that, silica particle size increases rapidly with silica loading [154].

It is found that increase in filler content reduces the strength of three polyethylenes (PE) filled with $CaCO_3$ with an average particle diameter of 2.3 μm [32]. The tensile strength of the ternary polymer composites, polyamide 6,6 (PA 6,6)/maleated poly[styrene-*b*-(ethylene-*co*-butylene)-*b*-styrene] (SEBS)/glass beads, is reduced by addition of glass beads [33]. Table 4, however, shows the tensile strength of glass bead filled epoxies increasing with filler loading [23]. Also, the strength of hybrid particulate epoxy composites with various glass bead loading and different rubber content increases with the amount of glass beads (whose size varies from 3 to 70 μm) [155]. But, it is observed that the strength of low density polyethylene (LDPE)/glass bead composites is insensitive to weight fraction of the beads (whose diameter varies from 1.4 μm to 116 μm) [31].

Table 4
Tensile strength of epoxy composites filled with glass beads (GB) with particle sizes in the range 4–44 μm at room temperature. Adapted from [23]

Material	Tensile strength (MPa)
Epoxy matrix	108
10 vol% GB	113
20 vol% GB	119
30 vol% GB	128

Fig. 20 plots the tensile strength of PU/nanosilica composite films against silica loading [156]. There is a large increase in strength even at very low silica content regardless of *in situ* polymerization or blending. Also, the tensile strength is higher by *in situ* polymerization than by blending because at the same filler wt% the former method results in more polyester chains chemically bonded to nanosilica that are more homogeneously dispersed in the polymer matrix.

The tensile strength of polyvinyl chloride (PVC)/nano-$CaCO_3$ nanocomposites at various weight ratios was studied [24]. At a weight ratio of 95/5, the nanocomposite exhibits a slightly higher tensile strength than neat PVC, indicating that the nanoparticles have enhanced the strength of the PVC matrix. However, further increase in nano-$CaCO_3$ particle loading decreases the tensile strength. This is explained by the poor filler–polymer interaction. Thus, nano-$CaCO_3$ particles are surface modified with chlorinated polyethylene (CPE) by preparing the CPE/nano-$CaCO_3$ master batch, which functions to strengthen the interaction between PVC and nano-$CaCO_3$. As a result, the strength is enhanced but only partially.

To summarize, the strength of particulate composites is determined not only by particle size and particle/matrix interfacial adhesion but also by particle loading. Various trends of the effect of particle loading on composite strength have been observed due to the interplay between these three factors, which cannot always be separated.

3.2. Theories for strength

The ultimate strength of a composite depends on the weakest fracture path throughout the material. Hard particles affect the strength in two ways. One is the weakening effect due to the stress concentration they cause, and another is the reinforcing effect since they may serve as barriers to crack growth. In some cases, the weakening effect is

predominant and thus the composite strength is lower than the matrix; and in other cases, the reinforcing effect is more significant and then the composites will have strengths higher than the matrix.

Prediction of the strength of composites is difficult. The difficulty arises because the strength of composites is determined by the fracture behaviours which are associated with the extreme values of such parameters as interface adhesion, stress concentration and defect size/spatial distributions. Thus, the load-bearing capacity of a particulate composite depends on the strength of the weakest path throughout the microstructure, rather than the statistically averaged values of the microstructure parameters. Hence, although numerous theories of composite strength have been published before, there is no universally accepted theory todate. In what follows, we summarize some phenomenological models and semi-empirical equations available because they are simple and easy to use in practice and can give correct predictions for appropriate cases.

Assuming that the stress cannot be transferred from the matrix to the filler and that the strength of a particulate-filled polymer composite is determined from the effective sectional area of load-bearing matrix in the absence of the particles, a very simple expression for the composite strength is given by [34,35]

$$\sigma_c = \sigma_m(1 - V_p) \tag{17}$$

where σ_c and σ_m are, respectively, composite strength and matrix strength, and V_p is particle volume fraction. Eq. (17) was proposed for poorly bonded particles. This equation indicates that the strength of a particulate composite decreases linearly with increasing particle loading. However, test results have shown that the relationship between σ_c and V_p is not always linear even if a decreasing tendency was observed. A modified form of Eq. (17) is thus obtained by replacing the particle volume fraction by a power law function of the volume fraction as [36,37]

$$\sigma_c = \sigma_m(1 - aV_p^b) \tag{18}$$

where a and b are constants depending on particle shape and arrangement in the composite. Eq. (18) still predicts a decrease in strength with increase of particle loading.

For poorly bonded particles, Nielsen's equation is often used for the prediction of strength of particulate composites. For cubic particles embedded in a cubic matrix, Nielsen gave [157]

$$\sigma_c = \sigma_m(1 - V_p^{2/3})Q \tag{19}$$

where the parameter Q accounts for weaknesses in the structure caused by the discontinuities in stress transfer and generation of stress concentration at the particle/polymer interface. When there is no stress concentration, the value of Q will be the maximum equal to unity.

Based on the hypothesis that there is no adhesion between filler and polymer, that is, the load is sustained only by the polymer, Nicolais and Nicodemo [158,159] derived, with simple geometric considerations, the following expression:

$$\sigma_c = \sigma_m(1 - 1.21V_p^{2/3}) \tag{20}$$

which gives a lower-bound strength of the composite. An upper-bound is immediately obtained by considering that, for perfect adhesion, the strength of the composite is simply equal to the strength of the polymer matrix. So, the strength is intermediate between these two bounds and cannot be higher than that of the matrix.

Jancar et al. [160] believed that stress concentration depends on particle volume fraction and presented a modified form of Eq. (20) as

$$\sigma_c = \sigma_m(1 - 1.21V_p^{2/3})S_r \tag{21}$$

where S_r is a strength reduction factor and varies in the range from 1.0 to 0.2 for low and high volume fractions, respectively.

Leidner and Woodhams [161] considered the contributions of particle/matrix friction and residual pressure to the composite strength and gave a modified equation

$$\sigma_c = 0.83pfV_p + k\sigma_m(1 - V_p) \tag{22}$$

where p is pressure, f is friction coefficient, and k is relative change in strength of matrix due to the presence of the filler. The first term on the right side of Eq. (22) is the friction contribution.

When some adhesion exists between particle and matrix, the interface can transfer a part of the stress to the particles, making a contribution to the composite strength. Thus, Eq. (18) may be modified for better prediction of composite strength as [162]

$$\sigma_c = \sigma_m(1 - aV_p^b + cV_p^d) \tag{23}$$

where c and d are constants. Eq. (20) can also be modified to include cases with some adhesion so that [163]

$$\sigma_c = \sigma_m(1 - 1.07V_p^{2/3}) \tag{24}$$

Piggott and Leidner [164] argued that the assumption of uniform filler distribution in most models was unlikely in practice and then proposed an empirical equation below

$$\sigma_c = g\sigma_m - \alpha V_p \tag{25}$$

where α is coefficient of the particle/matrix adhesion, and g is a constant.

It can be seen that in the case of nil or some adhesion, addition of particles generally leads to reduction in strength. But in the case of strong filler–matrix adhesion, where the stress is transferred through shear from the matrix to the particles, Eq. (22) can be rewritten as [161]

$$\sigma_c = 0.83pfV_p + k\sigma_m(1 - V_p) + \sigma_a H(1 - V_p) \tag{26}$$

where σ_a is the particle/matrix adhesion strength and H is a constant.

Furthermore, for very strong particle–matrix interfacial bonding, Pukanszky et al. [165,166] gave an empirical relationship

$$\sigma_c = \left[\frac{1 - V_p}{1 + 2.5V_p}\sigma_m\right]\exp(BV_p) \tag{27}$$

where B is an empirical constant, which depends on the surface area of particles, particle density and interfacial bonding energy. For poor interfacial bonding, the particles do not carry any load, so $B = 0$ [165,167]. Eq. (27) has been applied to analyse the strength results of epoxy/glass bead composites in which glass beads were subject to different treatments [23]. As shown in Fig. 21, B increases from 3.49 to 3.87 when the adhesion is improved by silane treatment of the glass beads compared to the untreated composites.

There have been a few attempts to correlate the strength of particulate composites with the diameter of the particle, d_p. An empirical linear relationship between composite strength and particle size was proposed [168], which is

$$\sigma_c = \sigma_m(1 - V_p) - k(V_p)d_p \tag{28}$$

where $k(V_p)$ is the slope of the tensile strength against the mean particle size (diameter) and is a function of particle volume fraction V_p. It can be easily seen that Eq. (28) is an extension of Eq. (17) with an additional negative term on the right side and it predicts a significant reduction in strength by adding particles. So, it is applicable to poorly bonded micro-particles but cannot be applied to strong interfacial adhesion, especially for nanocomposites. In addition, Hojo et al. [169,170] found that the strength of silica-filled epoxy decreased with increasing mean particle size d_p according to the relation

$$\sigma_c = \sigma_m + k_p(V_p)d_p^{-1/2} \tag{29}$$

where $k_p(V_p)$ is a constant being a function of the particle loading.

Young and Beaumont [26] also proposed a relation between strength and average interparticle distance D_s:

$$\sigma_c = \sigma_m + S/D_s \tag{30a}$$

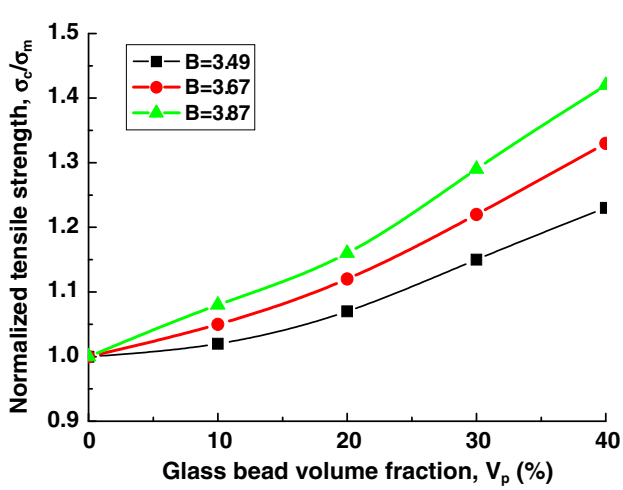

Fig. 21. Normalized tensile strength of glass bead filled epoxy composites versus the volume fraction of glass beads: (▽) untreated glass, (●) silane treated and (■) elastomer coated. Adapted from [23].

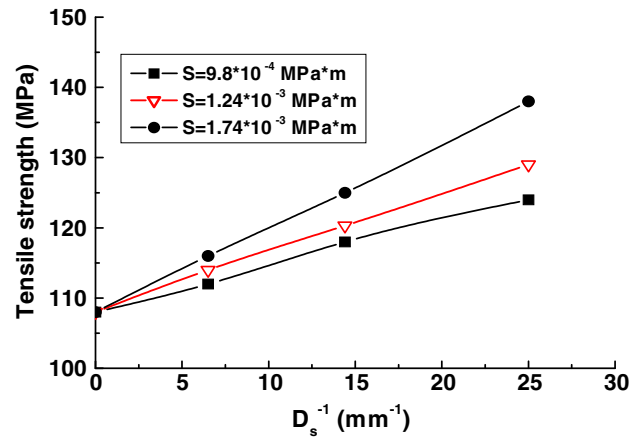

Fig. 22. The tensile strength of glass bead filled epoxy composites versus the average interparticle distance, $1/D_s$: (▽) untreated glass, (●) silane treated and (■) elastomer coated. Adapted from [23].

where S is a constant. D_s can be expressed as

$$D_s = 2d_p(1 - V_p)/3V_p \tag{30b}$$

Eqs. (29) and (30) predict the same trend that composite strength increases with decreasing particle size, as is consistent with published experimental data. For example, Fig. 22 shows that the effect of interparticle distance, D_s, on strength, σ_c, of an epoxy/glass bead composite [23] can be fitted very well to Eq. (30). Note that S depends on interface adhesion and varies from 9.8×10^{-4} to 1.74×10^{-3} MPa m.

Li et al. [171] developed a model that includes the effects of particle/matrix adhesion, particle size distribution, matrix degradation, etc. But the final expression of integration/summation is difficult to use in practical prediction of composite strength. Moreover, there is another disadvantage that the model is unsuitable for prediction of the strength of nanocomposites because it predicts a constant strength for particle sizes in nanoscale. To show the effect of particle size, two cases are considered [171]. In the first case ($n_p = 1$), the particles are perfectly bonded to the matrix and no degradation of matrix is assumed. In the second case ($n_p = 1 - V_p$), perfect bonding between particles and matrix is also used, but the matrix is assumed to degrade linearly with inclusion of particles due to the presence of particles and complications developed during the preparation of the composite. Using composite properties [171]: for glass particles – Young's modulus = 71 GPa, bulk modulus = 53.3 GPa, Poisson's ratio = 0.279, and epoxy – Young's modulus = 3.53 GPa, bulk modulus = 4.21 GPa, Poisson's ratio = 0.35 and tensile strength = 80 MPa, the effect of particle size on tensile strength is shown in Fig. 23 (where d_p is mean particle size). It is clear that composite tensile strength increases as particle size decreases; this effect is more pronounced for larger particles. This suggests that when the particle size is relatively large, reducing its size is very effective to improve the tensile strength of the composites. But if the particle size is

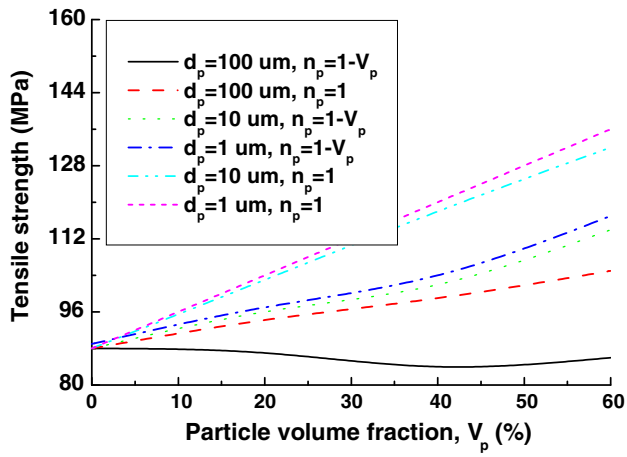

Fig. 23. Effect of particle size on the tensile strength of particulate-filled composites. Adapted from [171].

already small, further reducing its size is ineffective to enhance the composite strength. This conclusion is valid for the micro-composites considered in Fig. 23 but it does not apply to nanocomposites since the nanoparticle size effect is very significant on strength as shown by many results mentioned above.

In summary, strength of particulate–polymer composites relies on the parameters of particle size, interface adhesion and particle loading. Whilst many phenomenological and semi-empirical models have been proposed, there is no single equation that can apply to all particulate composites under all conditions. However, these models can predict the changing tendency of the strength against any specific parameter.

4. Fracture toughness

Fracture mechanics concept to material design considers the effects of cracks and defects on strength. Strength concept works with critical stresses but in fracture mechanics the critical crack length is an extra parameter. There are two approaches to determine fracture toughness which is a material property: stress intensity approach and energy approach. The first approach yields a fracture toughness (K_c) which relates the crack size to fracture strength. The energy approach provides a critical energy release rate (G_c) which is the work dissipation required to spread a crack of unit area. For non-linear elastic materials, the critical J-integral is used instead of G_c which is for linear elastic materials. Further discussions on these fracture analyses and related topics can be found in Atkins and Mai [172].

The expressions for K_c and its relation to G_c are originally derived for homogeneous, isotropic materials. Corrections for anisotropy have been given by Sih et al. [173]. However, these equations can be applied to particle-filled composites provided that the heterogeneities are very small compared to specimen dimensions and crack length. Under these conditions, G_c and K_c are connected by

$$G_c = K_c^2/E_c \tag{31}$$

where E_c is effective composite modulus. It will be shown that the fracture toughness, G_c and K_c, measured macroscopically is affected by particle size, interfacial adhesion and particle loading.

Michler [174] and Nakamura and Yamaguchi [175] examined micromechanical methods to study the deformation and fracture characteristics of toughened polymers and addressed the interrelationships between microstructure or morphology and mechanical properties. Fracture toughness depends on loading conditions, such as rate and temperature. So, the dependence of toughness on microstructural parameters, e.g. particle loading, is expected to be affected by both loading rate and temperature.

In ductile matrices, particulate fillers increase the brittleness of composites if there is no or little interfacial adhesion. In brittle matrices, the reverse holds and the brittleness is reduced. Micro-cavitation and micro-debonding can easily occur (see Fig. 24) and can introduce cracks of considerable sizes [151]. Design against brittle failure in composites is of critical importance.

Such transition from brittle to ductile fracture is already important for the bulk polymer material and it is influenced by internal and external conditions. Important external parameters are loading speed, notch radius and specimen thickness. The effects of these parameters were discussed and modelled by Brown [176]. Of special importance is the fact that the crack moves through areas in the middle of the specimen where plane strain prevails and at the surface where plane stress exists. The plane stress regions are able to yield and thus have a large crack resistance.

In the discussion of toughness of filled polymers these effects are superimposed to the effect of the inclusions on the modification of the polymer's bulk properties. To improve the toughness of the composite it is important that, in between the particles, regions with plane stress should be provoked that allows the material to yield. Thus,

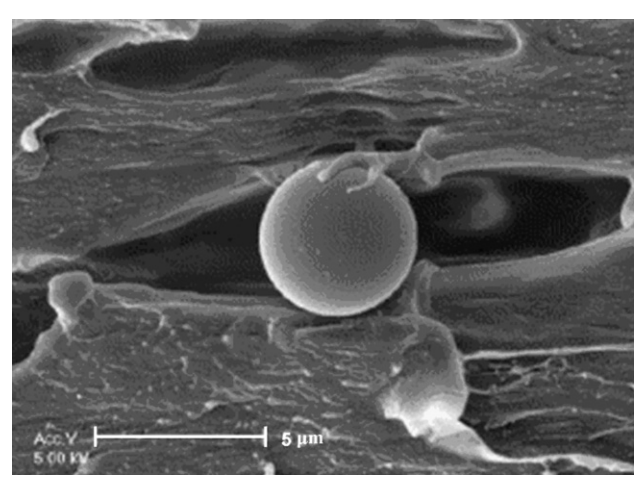

Fig. 24. Debonded glass particles surrounded by the void created due to deformation of the PP/glass composite. Adapted from [151].

a macroscopic brittle matrix may show localized plastic deformation or craze formation. This point has been addressed in calculating the fracture toughness of polypropylene blends [177] and glass sphere filled epoxy composites [178].

4.1. Experimental results

4.1.1. Effect of particle size

It will be shown below that the effect of particle size on composite fracture toughness is significant.

The fracture toughness (K_c) and critical energy release rate (G_c) of cured epoxy resin filled with 55 and 64 wt% angular-shaped silica particles prepared by crushing fused natural raw silica were studied over a range of particle size (2–47 μm) [175]. Both K_c and G_c values increase with increasing silica size and loading as shown in Figs. 25 and 26. The higher fracture toughness relative to the pure matrix was due to crack deflection around particles and energy dissipation in the damage zone.

Nakamura and Yamaguchi also studied the effect of particle size on the fracture behaviour of epoxy resin filled with five kinds of spherical silica particles prepared by hydrolysis of silicon tetrachloride having different mean sizes, ranging from 6 to 42 μm [179]. G_c and K_c were measured by single edge notched beam loaded in three-point bending (SENB-3PB), double torsion (DT) and Charpy impact tests. Both G_c and K_c increase with particle size at the same content though the improvements of DT and Charpy impact tests are smaller than SENB-3PB test due to different constraint effects on the crack-tip stresses. SEM study on the broken SENB-3PB specimens shows a smooth fracture surface with small particles ($d_p = 6$ μm) and a rough surface with large particles ($d_p = 42$ μm).

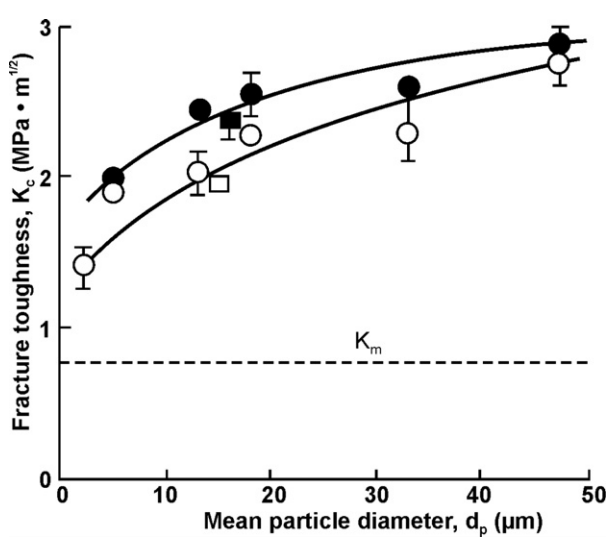

Fig. 25. Effect of particle size on the fracture toughness (K_c) measured by single edge notched bending (SENB) test of cured epoxy resins filled with classified angular-shaped silica particles at particle contents of 55 wt% (○) and 64 wt% (●), respectively. Broken line indicates the fracture toughness of unfilled cured epoxy resin. Adapted from [175].

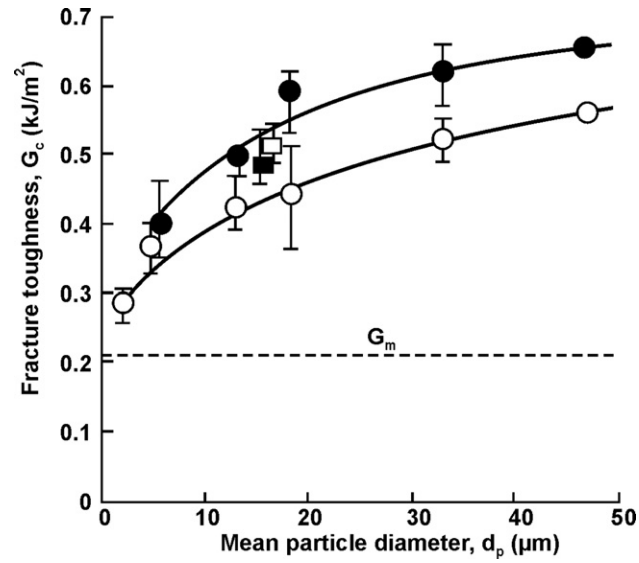

Fig. 26. Effect of particle size on the fracture toughness (G_c) measured by SENB test of cured epoxy resins filled with classified angular-shaped silica particles at particle contents of 55 wt% (○) and 64 wt% (●), respectively. Broken line indicates the fracture toughness of unfilled cured epoxy resin. Adapted from [175].

The latter is caused by crack deflections around large particles.

The particle size effect on fracture toughness, which is identical to G_c, of alumina trihydrate (ATH) filled epoxies was studied by Radford [21] and Lange and Radford [75] using a double-cantilever-beam (DCB) technique, and the results are shown in Table 5 and Fig. 27. Obviously, as the particle size d_p increases, so is G_c. But higher particle loading does not necessarily lead to higher toughness. Clearly, maximum toughness occurs at ~22 vol% particles and it decreases on either side of this point.

In the above, for composites with micron-size particles, fracture toughness increases with particle size. But there are exceptions as shown below, particularly when the particles are in the nanosize range and under high loading rates.

Fig. 28 shows the composite fracture toughness plotted against volume fraction of 20 μm, 3.5 μm and 100 nm aluminum particles added to polyester [74]. For the cases of 3.5 and 20 μm particles, the toughness increases monotonically with particle loading being more pronounced for the

Table 5
Fracture toughness of alumina trihydrate filled epoxies at room temperature. Adapted from [21]

Particle size, d_p (μm)	Fracture toughness, G_c (J m^{-2})	
	Volume fraction = 0.10	Volume fraction = 0.295
Unfilled	110.5	
1	130.9	67.7
2	–	75.4
5	–	124.2
8	182.9	177.6
12	243.7	197.2

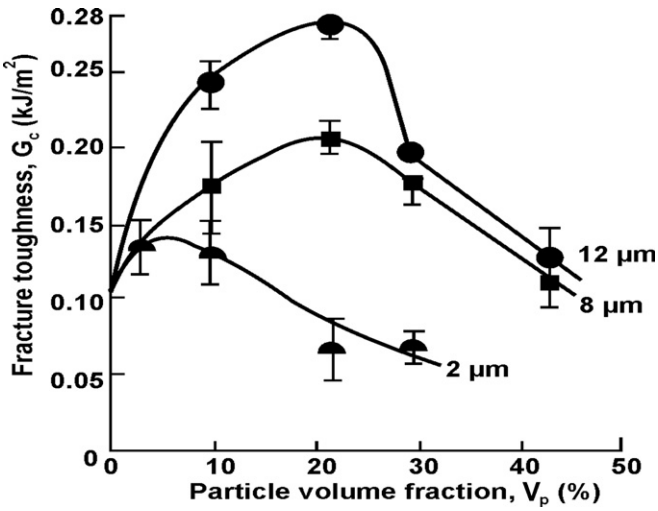

Fig. 27. Effects of particle size and volume fraction on the fracture toughness of alumina trihydrate powder filled epoxy composites at room temperature. Adapted from [75].

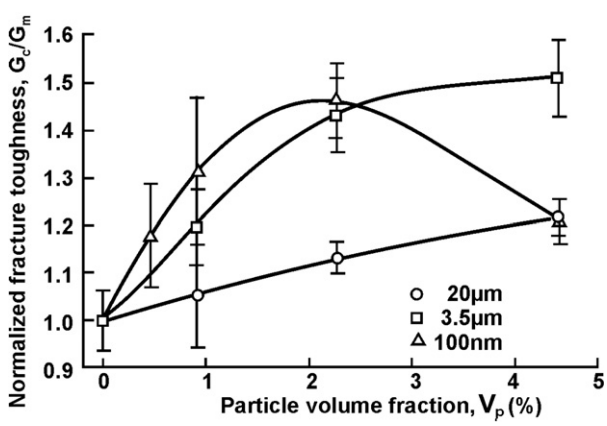

Fig. 28. Normalized fracture toughness of aluminum–polyester composites plotted against particle volume fraction for various particle sizes. Adapted from [74].

smaller particles. For example, at 4.4 vol% aluminum particles, the toughness increases by 51% and 22%, respectively, compared to neat polyester. Further reduction in particle size to 100 nm, a different trend is obtained, as shown in Fig. 28, in which the toughness has a maximum value at 2.3 vol% particles and decreases on either side of this loading.

The notched Izod impact toughnesss of polypropylene (PP)/$CaCO_3$ ($CaCO_3$ 1: 1 μm and $CaCO_3$ 2: 50 nm) composites and PP/elastomer (EOC, Dupont–Dow Chemical) blend as a function of the modifier content are shown in Fig. 29 [180]. In PP/EOC blends, there is a huge increase in the impact toughness as expected. The modification of PP with $CaCO_3$ particles also leads to toughness improvement but it depends strongly on the particle size. For example, adding 12 vol% 1 μm $CaCO_3$ to PP increases the impact toughness by merely 60% but this is very much larger at over 350% with the same loading of 50 nm $CaCO_3$ particles.

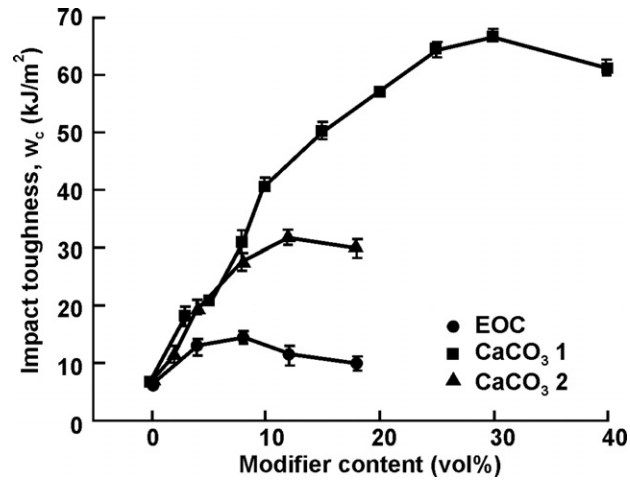

Fig. 29. Impact toughness of composites as a function of modifier content. Adapted from [180].

Under impact loading, when rigid calcium carbonate particles of three sizes (3.50, 0.70 and 0.44 μm) and varying volume fractions are added to high density polyethylene (HDPE) [57], the Izod toughness is also found to increase with decreasing particle size in the range studied.

To sum up the above observations, it is clear that particle size has an important effect on the composite toughness, which can be improved or reduced with increasing particle size. These results can be explained in terms of different operative toughening mechanisms in Section 4.2.

4.1.2. Effect of particle/matrix interfacial adhesion

The impact toughness of nylon 6/silica nanocomposites, in which most particle sizes fall in the range 50–110 nm, is shown in Fig. 30. A bell-shaped curve with a peak at 5 wt% particle is obtained and attributed to the evolution of microstructure [30]. The silica particles are treated by

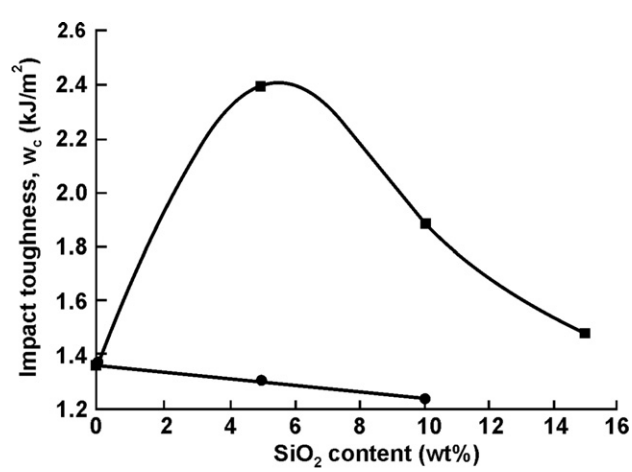

Fig. 30. Impact toughness of nylon 6 nanocomposites filled with modified (■) and unmodified (●) silica (SiO_2) particles, respectively. Adapted from [30].

amino-butyric acid to improve the particle/matrix adhesion. For untreated silica particles, the impact toughness decreases monotonically with increasing particle volume fraction probably due to the poor interfacial adhesion between silica and nylon 6 [30].

Three composites, PP/$CaCO_3$, PP/$CaCO_3$-1La and PP/$CaCO_3$-5La, in which $CaCO_3$ particles averaged ~40 nm modified with a lanthanum compound ($CaCO_3$-La) [181] and La_2O_3 concentrations of 0, 1 and 5 phr, respectively, were studied. The surface treatment improved the adhesion between particles and PP matrix. Fig. 31 shows the effects of $CaCO_3$, $CaCO_3$-1La and $CaCO_3$-5La concentrations on the notched Izod impact toughness of PP, which clearly points to peak values of 4.3, 6.6 and 7.9 kJ/m^2, respectively, at ~15 phr particle loading. Compared to the PP notched impact toughness of 2.6 kJ/m^2, these increases are significant for $CaCO_3$ treated by the lanthanum compound.

The beneficial effect on toughness of surface treated ultra-fine $CaCO_3$ particles (~70 nm) with stearic acid and a titanate coupling agent in PP over a range of concentration 0–40 vol% has also been confirmed [35]. Untreated particles decrease the toughness whereas a maximum, at 10 vol%, is observed for the treated particles. The crack-pinning model is used to analyse the fracture toughness but due to the very small size of particles the pinning contribution is proven to be negligible.

In contrast, for thermosetting matrices, increasing particle–matrix adhesion by using coupling agents does not give much enhanced toughness [22,38,42,59–62]. Crack growth is dominated by matrix failure and particle breakage. Thus, interface debonding is irrelevant and hence efforts to improve the interfacial adhesion are not effective to increase the toughness.

In general, therefore, interfacial adhesion between particles and matrix has a very significant effect on composite fracture toughness. Strong adhesion leads to high toughness in thermoplastic matrices but not necessary in thermosetting matrices due to different failure mechanisms.

4.1.3. Effect of particle loading

Alumina (Al_2O_3) nanoparticles with an average particle size of about 13 nm were added to an epoxy matrix [182] and their Charpy impact energies were determined as shown in Fig. 32. The results indicate strong enhancement of the impact toughness even at very low particle loadings of 0.5–2 vol%. There is a slight drop in toughness beyond 1 vol% but it is still larger than neat epoxy.

The effect of $CaCO_3$ ($d_p = 0.6$ μm) volume fraction (V_p) on the notched Izod impact toughness of HDPE/$CaCO_3$ composites with various w_a (equal to weight ratio of coupling agent (isopropyltriiso-stearoyl titanate) to $CaCO_3$ particles) is shown in Fig. 33 [183]. The impact toughness reaches a peak at 20 vol% and decreases with higher parti-

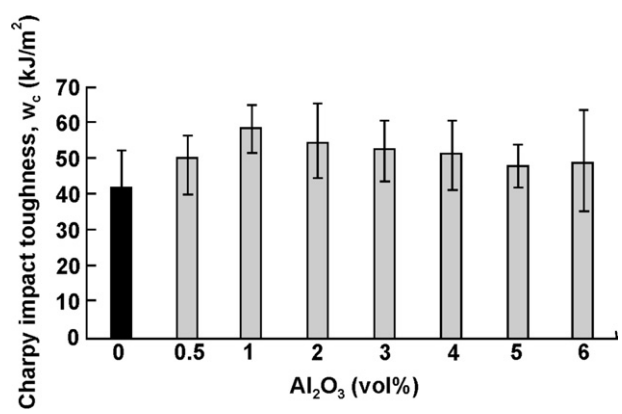

Fig. 32. Charpy impact toughness of epoxy/Al_2O_3 nanocomposites as a function of the filler content. Adapted from [182].

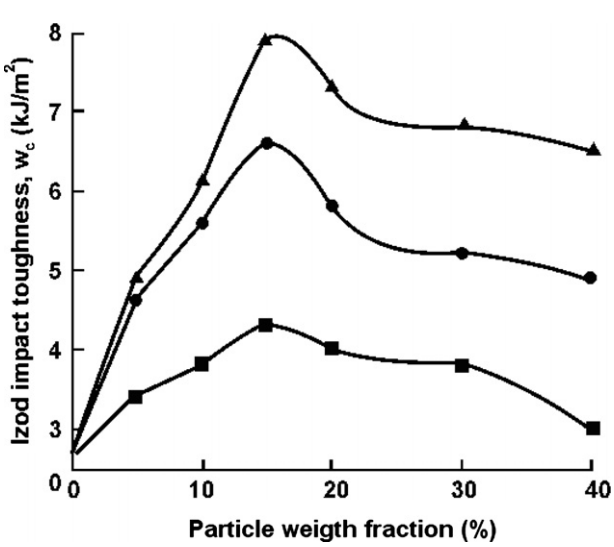

Fig. 31. Effect of the filler content on the impact toughness of PP/$CaCO_3$ composites: (■) $CaCO_3$, (●) $CaCO_3$-1La, and (▲) $CaCO_3$-5La. Adapted from [181].

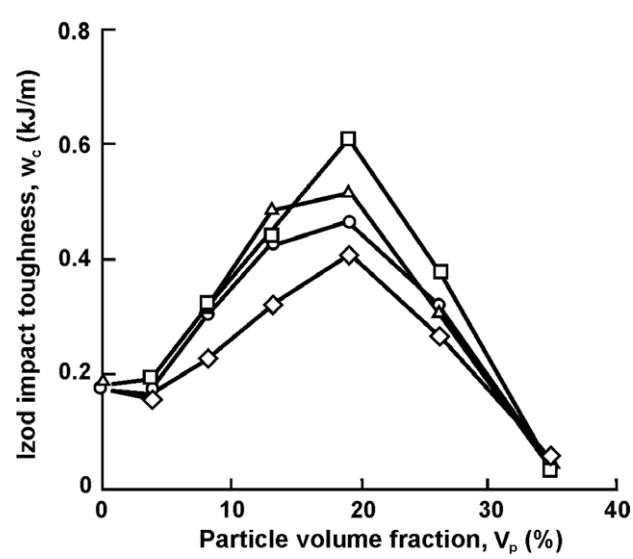

Fig. 33. Notched Izod impact toughness of HDPE/$CaCO_3$ composites ($d = 0.6$ μm) as a function of $CaCO_3$ volume fraction V_c. ○: $w_a = 0.025$; □: $w_a = 0.05$; △: $w_a = 0.075$; ◇: $w_a = 0.1$. Adapted from [183].

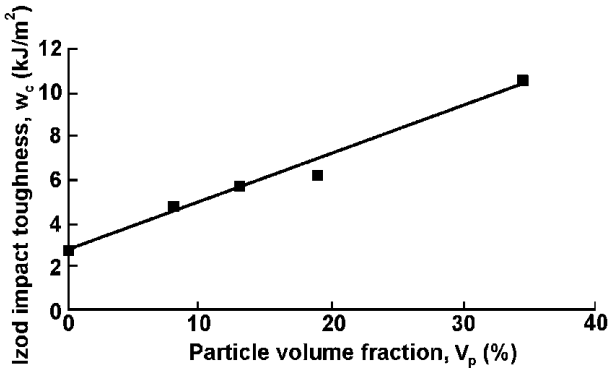

Fig. 34. Notched Izod impact toughness of $CaCO_3$/PP composites as a function of $CaCO_3$ particle content at 20 °C. Adapted from [184].

cle loading showing no toughening at ~30 vol%. The toughening efficiency also depends on w_a. A small amount of coupling agent ($w_a = 0.025$ and 0.05) gives rise to good dispersion of $CaCO_3$ particles and hence effective toughening of the composite. At higher w_a (=0.1), toughening is not as efficient probably due to the agglomeration of $CaCO_3$ particles [183].

Fig. 34 shows the effect of $CaCO_3$ particles with a diameter of 0.7 μm on the notched Izod fracture toughness of PP [184]. There is an almost linear increase and at 60 wt% (34.5 vol%) $CaCO_3$ the toughness is improved by fourfold. The toughening mechanisms are thought to be associated with debonding of particles. This prevents crazing of the polymer matrix and allows extensive plastic deformation, resulting in high fracture toughness. Without debonding there is no toughness increase.

The fracture energies (G_c) of unmodified and rubber-modified epoxies are plotted against the volume fraction of glass particles in Fig. 35 [63,185]. The inclusion of glass beads increases G_c of both materials but there is an optimal loading for maximum effect. For unmodified epoxy this occurs at $V_p = 0.3$ when G_c is increased by ~400%. For rubber modified epoxy, the optimum $V_p = 0.12$ at which G_c is increased by ~40%. Similar results are also reported by other authors. The fracture toughness of glass-filled epoxy and polyester resins was studied as a function of glass loading [59]. It was shown that toughness peaked at a medium glass loading (~30%) and decreased with more glass added. The fracture properties of ternary polymer composites: PA 6,6/maleated SEBS/glass beads were also studied in [33]. The average size of glass beads used was ~32 μm. It was found that the toughness reached a maximum at 5 wt% of glass beads and then decreased with more glass beads added.

The G_c results in Fig. 35b was re-plotted in Fig. 36 in terms of the fracture toughness K_c at the onset of crack growth at various temperatures [63]. K_c increases monotonically with glass loading and temperature. Addition of glass beads to epoxy matrix enhances K_c against fracture initiation.

Fig. 37 shows the improvement of fracture toughness K_c of epoxy by adding different types of particles. Clearly, K_c increases linearly with particle loading, which can be

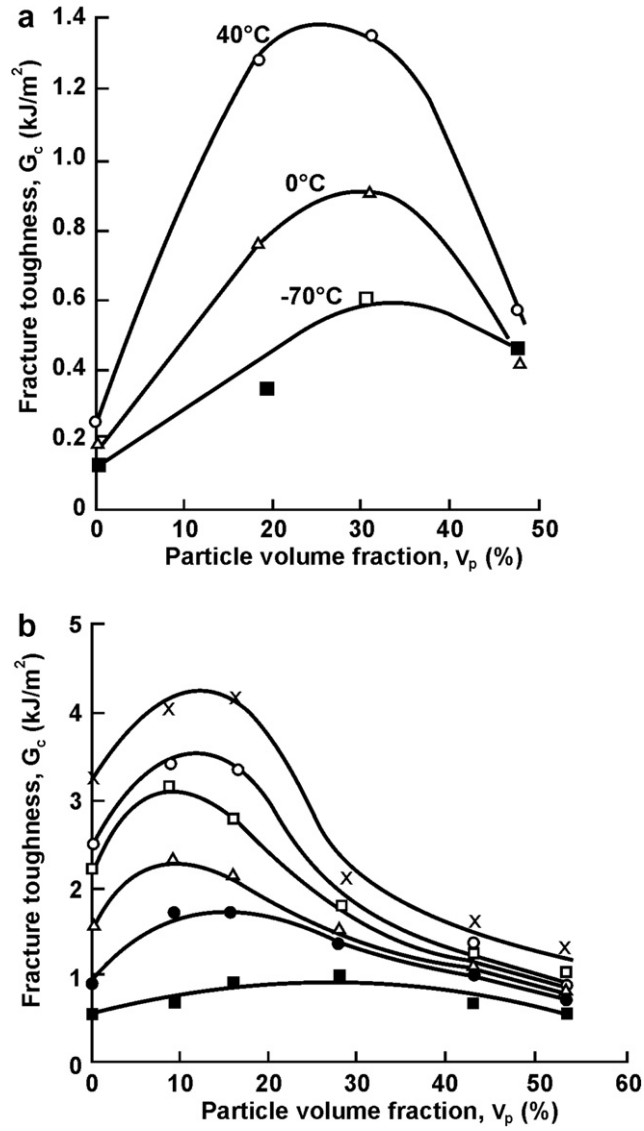

Fig. 35. Effect of glass loading V_p on fracture toughness G_c of glass bead filled epoxy composites. (a) Unmodified epoxy at the temperature of 40, 0 and −70 °C; and (b) rubber-modified epoxy at the temperature of 50, 40, 30, 0, −20 and −70 °C respectively from top to bottom. Adapted from [63,185].

related to the progressive increase in frequency of transparticle fracture [38,61]. The improvement due to the particles is in decreasing order: silicon carbide > silica > alumina trihydrate (ATH) > glass beads.

However, in ductile thermoplastics, it is observed that the addition of rigid particles often brings about a reduction in fracture toughness. Table 6 shows the fracture toughness G_c of calcium carbonate–polypropylene (PP) composites decreasing with increase of particle volume fraction [47].

4.2. Toughening mechanisms and theories for prediction of fracture toughness

There have been numerous experimental studies on toughening of particulate–polymer composites using inor-

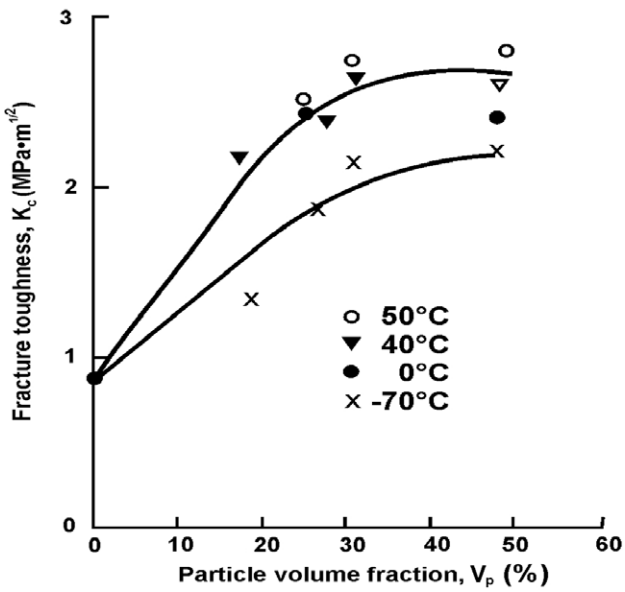

Fig. 36. Fracture toughness K_c of glass bead filled epoxy composites as a function of glass bead volume fraction v_p. Adapted from [63].

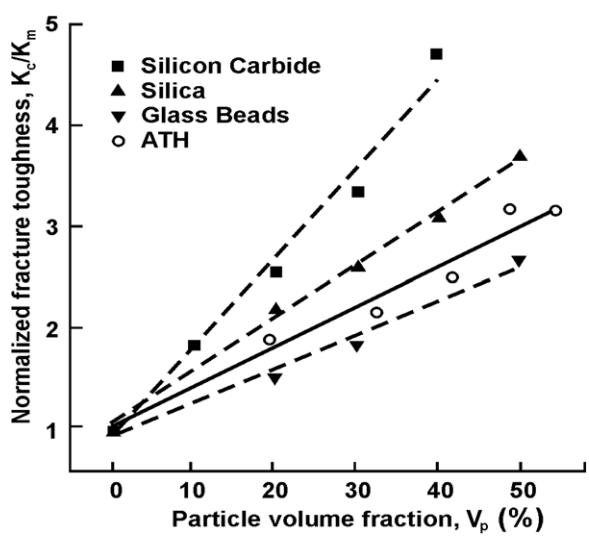

Fig. 37. Relationship between the normalized fracture toughness, $K_c(c)/K_c(m)$ and V_p for various glass bead loadings at different temperatures. Adapted from [38,61].

Table 6
G_c (kJ/m^2) of PP filled with $CaCO_3$ particles with average particle size of 3.6 μm. Adapted from [47]

Filler content	Strain energy release rate, G_c (kJ/m^2)
0	5.1
0.05	4.6
0.10	4.1
0.15	3.7
0.21	3.4
0.25	3.1
0.30	2.8

ganic particles. Many models have been published which are valuable to characterize the microstructure–property relationship, determine the key parameters that affect fracture toughness, reduce the number of necessary tests and provide guidance to design novel composites. Because of the complexity of damage and toughening mechanisms, few models apply to all composite systems. Some recent models are reviewed in [186–188] but as yet efficient models to provide reliable toughness predictions of particulate composites are wanting.

To-date, a range of possible toughening mechanisms have been proposed [22,35,189–200] and they include: (a) crack front bowing (or crack pinning), (b) crack-tip blunting, (c) particle–matrix interface debonding, (d) diffused matrix shear yielding, (e) micro-cracking, (f) crack deflection by hard particles, (g) micro-shear banding, and (h) breakage of particles, etc. Some of these toughening mechanisms may occur cooperatively in particulate composites; and many of them have already been discussed in a previous review paper [189]. It should, however, be noted that recently the plastic void growth model [195] and the 3-D interphase network model [196] were advocated as possible toughening mechanisms for epoxy/nanosilica composites. In the following, the first two toughening mechanisms of crack-pinning and crack-tip blunting are presented in more detail. As to other mechanisms, readers are referred to the appropriate references cited above.

The concept that crack pinning (bowing) could lead to increased fracture toughness was first postulated by Lange [43], subsequently refined by Evans [197] and later developed further by Green et al. [198,199] for different particle shapes. The concept is simple in that a crack pinned by two impenetrable particles needs more energy to propagate if its front is lengthened by bowing [195,199]. For weak particles, there is no crack bowing (and this will not be further considered).

In many studies [26,42,45,59,63,75,185,201,202], crack pinning (bowing) is considered a major mechanism for particle toughening. This offers simple but satisfactory explanations about the effect of particle loading. Accordingly, rigid particles pin down the crack and its front bows between them acting as anchors. The increase in line energy is akin to the line tension in dislocation pinning in metals. A characteristic feature of crack pinning is the "tails" left behind the particles [22,42,43,75,199,203]. The following simple model given by Lange [43] relates the fracture toughness G_c to the line tension T:

$$G_c = G_m + \frac{T}{D_s} \tag{32}$$

where D_s is interparticle spacing depending on particle diameter d_p and particle loading V_p defined by Eq. (13); and G_m is matrix toughness.

Combining Eqs. (32) and (30b) yields an equation which predicts that G_c should improve with increasing V_p for a given d_p. This is precisely what has been found for low volume fractions of filler [26,193,204]. But, for some brittle

matrix composites, G_c was found to reach a maximum at a critical V_p and then fall with further addition of particles. Another problem that arises with Eq. (32) is that when G_c is plotted against $1/D_s$ for different sizes of particles in a given brittle matrix, lines of different initial slope are obtained [192,204]. This clearly implies that the line tension, T, is a function of particle size. Lange [203] introduced a non-dimensional parameter $F(d_p)$ to Eq. (32) to overcome this problem. That is,

$$G_c = G_m + \frac{F(d_p)T}{D_s} \tag{33}$$

where $0 \leqslant F(d_p) \leqslant 1$. However, this modification is not satisfactory and the physical meaning of $F(d_p)$ is unclear. Moreover, Eq. (33) always predicts a higher composite toughness G_c than matrix toughness G_m. This contradicts many experimental results especially those for ductile polymer matrix composites. Lange's equations also predict that, for a given V_p, small particles d_p should give better toughening. This was not supported by experimental results [21,35,175]. Lange assumed a flat surface in his model, but the fracture plane is always quite rough [21,59] implying high surface energy absorption to the total composite toughness.

Lange's modification [75,203] was improved by Evans [197], Green et al. [198,199,205] and Rice et al. [206–208]. Using Lange's line tension concept, Evans [197] and Rice et al. [206–208] expanded the line energy calculations for various particle configurations, which explain the dependence of composite toughness on interparticle separation, particle size, bowed crack shape and interaction between bowed cracks. Green et al. [198,199,205] suggested that the impenetrability of particles might depend on various factors: size, loading, toughness of particles, interfacial adhesion, coefficients of thermal expansion and elastic modulus mismatch. According to the modified crack bowing theories, the line energy or the stress for crack growth depends on the ratio of particle size and interparticle spacing. This ratio is a function of particle volume fraction. Hence, line tension, size and volume fraction of particles can be interrelated, namely $T = T(V_p, d_p, D_s)$. However, quantitative prediction of toughness is still difficult because the effects of interfacial bonding strength, strain rate on matrix and other material variables have not been included in the revised models. Using the modified theory of Green et al. [198,199,205], Spanoudakis and Young [22,42] predicted the fracture toughness of glass bead filled epoxies in reasonable agreement with test results.

In addition to the crack-pinning mechanism, crack-tip blunting was proposed as another underlying mechanism for glass bead filled epoxies, since the strain rate dependence of toughness could not be understood by crack pinning alone [22,42]. For unmodified epoxy filled with glass beads, crack pinning is the main toughening effect [155] strongly supported by "tails" behind the particles on the fracture surface and Eq. (33) fits the experimental data well. For the rubber-modified epoxy filled with glass beads, crack pinning cannot explain the high values of G_c or K_c since crack-tip blunting is involved [155]. The effects of strain rate and temperature on crack-tip blunting and hence toughness of unmodified and rubber-modified epoxies filled with zirconia particles (<1 μm) were studied by Low and Mai [209]. Two crack-tip blunting mechanisms were proposed: (a) thermal blunting caused by adiabatic heating at the crack tip; and (b) plastic blunting due to shear yielding. Crack-tip blunting also affected the crack growth characteristics of these materials, e.g. stick-slip and stable growth [210]. Kinloch and Williams [211] suggested that plastic blunting is favoured when the epoxy yield stress is lower than 100 MPa.

Damage mechanics indicates that the energy required to fracture a material is related to its effective load-bearing area [212,213]. For poorly bonded particulate composites, the crack-pinning mechanism may not apply. Bucknall [214] assumed that all dissipated energies during fracture are absorbed by the matrix material and the unbonded beads reduce the effective load-bearing area. Using the effective area model developed by Ishai and Cohen [215] and Nicolais and Narkis [159], the composite toughness was estimated by [186]

$$G_c = G_m(1 - 1.21V_p^{2/3}) \tag{34}$$

which applies to the toughness results of some glass bead–poly(phenylene) oxide composites but some pronounced errors are also found compared to other test data. Zebarjad et al. [216] studied the influence of weakly bonded $CaCO_3$ particles on the deformation and fracture mechanisms in PP/$CaCO_3$ composites with three-point bend tests and found the toughness of PP decreased with increasing $CaCO_3$ loading (Fig. 38). These results are consistent with Eq. (34).

It is noted that Eq. (34) assumes that the crack propagates through the minimum cross-sectional area of the matrix and that the particles do not influence the fracture process. These assumptions are inappropriate for most real composites, and hence it often underestimates G_c. To

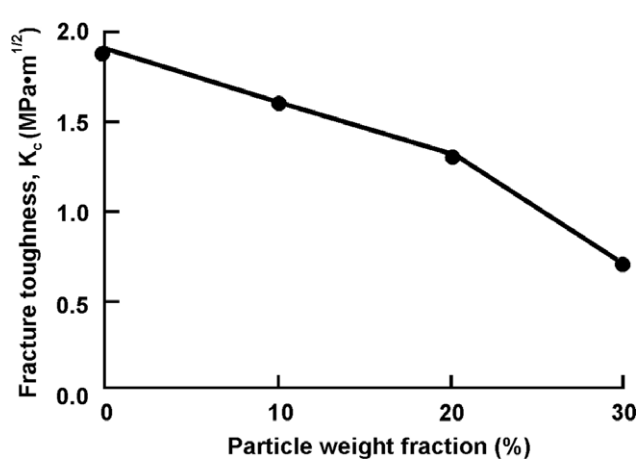

Fig. 38. Dependency of fracture toughness K_c of polypropylene (PP) composite on calcium carbonate content. Adapted from [216].

redress this problem, Kendall [46] assumed that when a crack meets a particle, it will grow along the particle/matrix interface whose fracture toughness is G_f. Then considering the extra area of fracture surface due to the presence of particles, he obtained the relation below to calculate the composite fracture toughness:

$$G_c = G_m(1 - k_\phi) + G_f n k_\phi \tag{35}$$

where k_ϕ is enhanced fracture surface volume fraction, which depends on the fracture path, and n takes into account the extra path around the particles. Eq. (35) without the second term on the right side, since this is thought to be negligible, has been used by Friedrich and Karsch [217] to describe the toughness of a series of silica–PP composites with good accuracy. Naturally, these two models assume no or weak adhesion between particles and matrix and hence predict toughness to decrease with particle loading.

Lange and Radford [75] studied the fracture of alumina trihydrate (ATH) filled epoxy resins and reported that G_c was improved by adding the particles. This was attributed to crack pinning. They used three different median particle sizes: 1, 8 and 12 μm (see Fig. 27). As the particle size increased, the peak value G_c also increased. They explained this by assuming large particles were better able to support crack pinning than small particles, and thus more efficient in improving the overall G_c. Conversely, the decrease in G_c beyond the peak value suggests a reduced extent of crack pinning at high volume fractions. Furthermore, crack blunting was concluded to be the dominant toughening mechanism for large ATH particles because the particles were weak, frequently undergoing cleavage and unstable to participate extensively in crack pinning. For most particles, the higher the particle strength, the larger the enhancement of fracture toughness achieved per unit volume fraction. The leveling of K_c sometimes observed at high volume fractions may be due to an increase in the frequency of trans-particle fractures.

The mechanism of crack interaction with a second phase dispersion is qualitatively consistent with the results obtained by Lange and Radford [75] where two different types of fracture surfaces were observed. One type included surface steps associated with each particle encountered by the moving crack front. They are a characteristic feature of the interaction of a crack with inhomogeneities, such as voids and second phase particles. This type of surface was only observed for composites containing dispersed phase volume fractions smaller than that resulting in peak toughness. The second type of surface appeared similar to that of polycrystalline materials. Such surfaces were found for composites with volume fractions larger than that yielding peak toughness. A combination of both types of fracture surfaces was observed for composites with peak toughness. In general, for large interparticle spacing, a surface containing steps was observed. For small interparticle spacing, the surface appeared polycrystalline. During fracture, a moving crack is momentarily pinned at positions of inhomogeneities within the brittle matrix. This interaction leads to crack front bowing, thus increasing its total length when the particle spacing decreases and the line tension rises. However, a maximum is reached inferring that the dispersed particles become too closely spaced to interact effectively with the crack front. Smaller particles are less effective as anchors than larger particles. Therefore, the fracture toughness is higher for the composite containing larger particles.

Particle/matrix interface adhesion was found to affect both the crack growth behaviour and the appearance of the fracture surface of glass bead filled epoxy micro-composites [42]. The main toughening mechanism is crack pinning. For poorly bonded particles, the crack is attracted to the equators of the particles and moves around the particles. The fracture surface consists of hemispherical holes and top surfaces of debonded particles. For well-bonded particles, the crack is attracted to the poles of the particles. The crack then propagates through the matrix above or below the particles leaving a layer of epoxy resin covering them.

Weak interfacial adhesion between rigid particles and matrix makes crack pinning less effective because debonded particles are ineffective as pinning sites [63]. Moreover, Levita et al. [35] reported that the crack-pinning contribution to G_c is negligible for very small particle size. Small particles differ from coarse ones if the interface adhesion affects the composites properties (since surface to volume ratio increases with reciprocal particle size). If interfacial debonding dominates, smaller particles will lead to larger G_c due to their higher total surface area than larger particles at a given volume fraction.

As mentioned above, another approach to explain the toughness variation of particle-filled polymers is based on the fracture process zone concept. Evans et al. [218] argued that energy dissipation processes within a dissipation zone in front of the crack are responsible for toughness enhancement by adding hard particles to ductile polymers. They found that particle debonding and subsequent yielding of local polymer regions are the dominant mechanisms. Similar argument was used by Bohse et al. [219].

The toughening mechanisms of semi-crystalline polymers (e.g., polyamides and isotactic polypropylene) reinforced with rubber particles have been extensively studied [220–224]. The effects of such parameters as rubber particle size, volume fraction and interparticle distance on the effectiveness of toughening have been examined. It has been concluded [222] that for a blend to be tough, the particles must be smaller than a critical size, which depends on the matrix type and rubber concentration. Similarly, rubber concentration must be above a critical level that, in turn, is a function of particle size. Based on experimental observations of a series of rubber-modified polyamide-6,6 blends, Wu [225,226] found that the thickness of the matrix ligaments between rubber particles is a key parameter for rubber toughening. He noted that a sharp brittle–tough transition occurs when the average thickness of the matrix ligaments is smaller than a certain critical value. Several

explanations for this phenomenon were proposed by Wu, but rejected by Muratoglu et al. [227] who concluded that the change of the local matrix structure caused by the inclusions is responsible for the change of toughness. This idea was extended and proven for certain semi-crystalline polymers in subsequent papers [222,228]. The primary role of the filler is to introduce a high amount of interface that affects the crystallization process and modifies the structure of the polymer in the neighborhood of the particle surface. The role of the trancrystalline regions due to nanosized soft and hard particles, such as rubber and clay, on toughness has been recently studied by Dasari et al. [229].

5. Concluding remarks

A critical review of the experimental results and theories of the mechanical properties including modulus, strength and fracture toughness of polymer based particulate micro- and nano-composites is presented. The effects of particle size, particle/matrix adhesion and particle loading on composite stiffness, strength and toughness of a range of particulate composites having both micro- and nano-fillers with small aspect ratios of unity and thereabout are examined in detail. It is shown that composite strength and toughness are strongly affected by all three factors, especially particle/matrix adhesion. This is expected because strength depends on effective stress transfer between filler and matrix, and toughness/brittleness is controlled by adhesion. Various trends of the effect of particle loading on composite strength and toughness have been observed due to the interplay between these three factors, which cannot always be separated. However, composite stiffness depends significantly on particle loading, not particle/matrix adhesion, since the fillers have much larger modulus than the matrix. There is also a critical particle size, usually in nanoscale, below which the composite stiffness is greatly enhanced due to the significant effect of the particle size, probably caused by the much larger surface areas imparting a "nano"-effect. A critical evaluation of existing test data and available theoretical and phenomenological models is given to obtain basic knowledge of the strengthening, stiffening and toughening mechanisms in these particulate composites. The applicability of existing models, both phenomenological and empirical/semi-empirical, to describe the experimental results for polymer-based particulate composites are discussed.

Acknowledgements

Financial support from the National Natural Science Foundation of China (Grant Nos.: 50573090, 10672161, 10525210 and 10732050), the Overseas Outstanding Scholar Foundation of the Chinese Academy of Sciences (Grant Nos.: 2005-1-3 and 2005-2-1), the 973 Project (2003CB615603), the Australian Research Council and the Alexander von Humboldt Foundation is gratefully acknowledged.

References

[1] Ray SS, Okamoto M. Polymer/layered silicate nanocomposites: a review from preparation to processing. Prog Polym Sci 2003;28:1539–641.
[2] Alexandre M, Dubois P. Polymer-layered silicate nanocomposites: preparation, properties and uses of a new class of materials. Mater Sci Eng R 2000;28:1–63.
[3] Kim MH, Park CI, Choi WM, Lee JW, Lim JG, Park OO. Synthesis and material properties of syndiotactic polystyrene/organophilic clay nanocomposites. J Appl Polym Sci 2004;92:2144–50.
[4] Liu L, Qi Z, Zhu X. Studies on nylon 6/clay nanocomposites by melt-intercalation process. J Appl Polym Sci 1999;71:1133–8.
[5] Usuki A, Kojima Y, Kawasumi M, Okada A, Fukushima Y, Kurauchi T, et al. Synthesis of nylon-6–clay hybrid. J Mater Res 1993;8:1179–83.
[6] Giannelis EP. Polymer layered silicate nanocomposites. Adv Mater 1996;8:29–35.
[7] Kojima Y, Usuki A, Kawasumi M, Fukushima Y, Okada A, Kurauchi T, et al. One-pot synthesis of nylon-6 clay hybrid. J Polym Sci Part A Polym Chem 1993;31:1755–8.
[8] Tyan HL, Liu YC, Wei KH. Thermally and mechanically enhanced clay/polyimide nanocomposite via reactive organoclay. Chem Mater 1999;11:1942–7.
[9] Shi H, Lan T, Pinnavaia T. Interfacial effects on the reinforcement properties of polymer–organoclay nanocomposites. Chem Mater 1996;8:1584–7.
[10] Cho JW, Paul DR. Nylon 6 nanocomposites by melt compounding. Polymer 2001;42:1083–94.
[11] Wang Z, Lan T, Pinnavaia TJ. Hybrid organic–inorganic nanocomposites formed from an epoxy polymer and a layered silicic acid (magadiite). Chem Mater 1996;8:2200–4.
[12] Zhang YH, Wu JT, Fu SY, Yang SY, Li Y, Fan L, et al. Studies on characterization and cryogenic mechanical properties of polyimide-layered silicate nanocomposite films. Polymer 2004;45:7579–87.
[13] Tjong SC. Structural and mechanical properties of polymer nanocomposites. Mater Sci Eng R 2006;53:73–197.
[14] Lau KT, Gu C, Hui D. A critical review on nanotube and nanotube/nanoclay related polymer composite materials. Composites Part B 2006;37:425–36.
[15] Xie XL, Zhou XP, Mai Y-W. Dispersion and alignment of carbon nanotubes in polymer matrix: a review. Mater Sci Eng R 2005;49:89–112.
[16] Zhu ZK, Yang Y, Yin J, Qi ZN. Preparation and properties of organosoluble polyimide/silica hybrid materials by sol–gel process. J Appl Polym Sci 1999;73:2977–84.
[17] Dekkers MEJ, Heikens D. The effect of interfacial adhesion on the tensile behavior of polystyrene–glass-bead composites. J Appl Polym Sci 1983;28:3809–15.
[18] Fu SY, Lauke B. Characterization of tensile behaviour of hybrid short glass fibre calcite particle ABS composites. Composite Part A 1998;29A:575–83.
[19] Fu SY, Lauke B. Analysis of mechanical properties of injection molded short glass fibre (SGF)/calcite/ABS composites. J Mater Sci Technol 1997;13:389–96.
[20] Eirich FR. Some mechanical and molecular aspects of the performance of composites. J Appl Polym Sci Appl Polym Symp 1984;39:93–102.
[21] Radford KC. The mechanical properties of an epoxy resin with a second phase dispersion. J Mater Sci 1971;6:1286–91.
[22] Spanoudakis J, Young RJ. Crack propagation in a glass particle-filled epoxy–resin. 1. Effect of particle-volume fraction and size. J Mater Sci 1984;19:473–86.
[23] Amdouni N, Sautereau H, Gerard JF. Epoxy composites based on glass-beats. 2. Mechanical-properties. J Appl Polym Sci 1992;46:1723–35.

[24] Wang M, Berry C, Braden M, Bonfield W. Young's and shear moduli of ceramic particle filled polyethylene. J Mater Sci Mater Med 1998;9:621–4.
[25] Hsueh CH. Effects of aspect ratios of ellipsoidal inclusions on elastic stress transfer of ceramic composites. J Am Ceram Soc 1987;72: 344–7.
[26] Young RJ, Beaumont PWR. Effect of composition upon fracture of silica particle-filled epoxy–resin composites. J Mater Sci 1977;12: 684–92.
[27] Pukanszky B, Voros G. Mechanism of interfacial interactions in particulate filled composites. Compos Interf 1993;1:411–27.
[28] Nakamura Y, Yamaguchi M, Okubo M, Matsumoto T. Effects of particle size on mechanical and impact properties of epoxy resin filled with spherical silica. J Appl Polym Sci 1992;45:1281–9.
[29] Reynaud E, Jouen T, Gauthier C, Vigier G, Varlet J. Nanofillers in polymeric matrix: a study on silica reinforced PA6. Polymer 2001;42:8759–68.
[30] Ou Y, Yang F, Yu ZZ. A new conception on the toughness of nylon 6/silica nanocomposite prepared via in situ polymerization. J Polym Sci Part B Polym Phys 1998;36:789–95.
[31] Liang JZ, Li RKY, Tjong SC. Tensile fracture behaviour and morphological analysis of glass bead filled low density polyethylene composites. Plast Rubber Compos Process Appl 1997;26:278–82.
[32] Chacko VP, Farris RJ, Karasz FE. Dynamic mechanical spectrometry of nylon-12. J Appl Polym Sci 1983;28:2701–5.
[33] Tjong SC, Xu SA. Ternary polymer composites: PA6,6/maleated SEBS/glass beads. J Appl Polym Sci 2001;81:3231–7.
[34] Danusso F, Tieghi G. Strength versus composition of rigid matrix particulate composites. Polymer 1986;27:1385–90.
[35] Levita G, Marchetti A, Lazzeri A. Fracture of ultrafine calcium carbonate/polypropylene composites. Polym Compos 1989;10: 39–43.
[36] Nicolais L, Narkis M. Stress–strain behavior of styrene–acrylonitrile/glass bead composites in the glassy region. Polym Eng Sci 1971;11:194–9.
[37] Nicolais L, Nicodemo L. Effect of particles shape on tensile properties of glassy thermoplastic composites. Int J Polym Mater 1974;3:229.
[38] Moloney AC, Kausch HH, Kaiser T, Beer HR. Review – parameters determining the strength and toughness of particulate filled epoxide resins. J Mater Sci 1987;22:381–93.
[39] Kinloch AJ, Young RJ. Fracture behavior of polymers. London: Elsevier Applied Science; 1983, p. 229.
[40] Shimbo M, Ochi M, Arai K. Internal stress of cured epoxide resin coatings having different network chains. J Coat Technol 1984;56:45–51.
[41] Shimbo M, Ochi M, Shigeta Y. Shrinkage and internal stress during curing of epoxide resins. J Appl Polym Sci 1981;26:2265–77.
[42] Spanoudakis J, Young RJ. Crack propagation in a glass particle-filled composite at or near a rigid spherical inclusion. J Mater Sci 1984;19:487–96.
[43] Lange FF. The interaction of a crack front with a second phase dispersion. Philos Mag 1970;22:983–92.
[44] Nielsen LE, Landel RF. Mechanical properties of polymers and composites. 2nd ed. New York: Marcel Dekker; 1994, p. 131–232.
[45] Rothon R. Particulate-filled polymer composites. New York: John Wiley & Sons; 1995.
[46] Kendall K. Fracture of particulate filled polymers. Brit Polym J 1978;10:35–8.
[47] Jancar J, Dibenedetto AT. Failure mechanics in ternary composites of polypropylene with inorganic fillers and elastomer inclusions. J Mater Sci 1995;30:2438–45.
[48] Fu SY, Lauke B. Fracture resistance of unfilled and calcite particle-filled ABS composites reinforced by short glass fibers (SGF) under impact load. Composite Part A 1998;29A:631–41.
[49] Pukanszky B. Composites. In: Karger-Kocsis J, editor. Polypropylene: structure, blends and composites, vol. 3. London: Chapman & Hall; 1995. p. 1–70.
[50] Baker RA, Koller LL, Kummer PE. Calcium carbonate. In: Katz HS, Milevski JL, editors. Handbook of fillers for plastics. 2nd ed. New York: Van Nostrand Reinhold Co; 1987. p. 119–42.
[51] Badran BM, Galeski A, Kryszewski M. High-density polyethylene filled with modified chalk. J Appl Polym Sci 1982;27:3669–81.
[52] Hoffmann H, Grellmann W, Zilvar V. Instrumented impact studies on thermoplastic composites. In: Sedlacek B, editor. 28th Microsymposium on macromolecules polymer composites. Polymer composites. New York: Walter de Gruyter; 1986. p. 233–42.
[53] Fu Q, Wang G. Polyethylene toughened by rigid inorganic particles. Polym Eng Sci 1992;32:94–7.
[54] Fu Q, Wang G, Shen J. Polyethylene toughened by $CaCO_3$ particles: brittle–ductile transition of $CaCO_3$-toughened HDPE. J Appl Polym Sci 1993;49:673–6.
[55] Fu Q, Wang G. Effect of morphology on brittle–ductile transition of HDPE/$CaCO_3$ blends. J Appl Polym Sci 1993;49:1985–8.
[56] Fu Q, Wang G. Polyethylene toughened by $CaCO_3$ particles-percolation model of brittle–ductile transition in HDPE/$CaCO_3$ blends. Polym Int 1993;30:309–12.
[57] Bartczak Z, Argon AS, Cohen RE, Weinberg M. Toughness mechanism in semi-crystalline polymer blends: II. High-density polyethylene toughened with calcium carbonate filler particles. Polymer 1999;40:2347–65.
[58] Sumita M, Shizuma T, Miyasaka K, Ishikawa K. Effect of reducible properties of temperature, rate of strain, and filler content on the tensile yield stress of nylon 6 composites filled with ultrafine particles. J Macromol Sci 1983;B22:601–18.
[59] Broutman LJ, Sahu S. The effect of interfacial bonding on the toughness of glass filled polymers. Mater Sci Eng 1971;8:98–107.
[60] Kinloch AJ. Structural adhesives. London: Elsevier Applied Science Publishers; 1986.
[61] Roulin-Moloney AC, Cantwell WJ, Kausch HH. Parameters determining the strength and toughness of particulate-filled epoxy resins. Polym Compos 1987;8:314–23.
[62] Sahu S, Broutman LJ. Mechanical properties of particulate composites. Polym Eng Sci 1972;12:91–100.
[63] Kinloch AJ, Maxwell DL, Young RJ. The fracture of hybrid–particulate composites. J Mater Sci 1985;20:4169–84.
[64] Alcock B, Cabrera NO, Barkoula NM, Reynolds CT, Govaert LE, Peijs T. The effect of temperature and strain rate on the mechanical properties of highly oriented polypropylene tapes and all-polypropylene composites. Compos Sci Technol 2007;67:2061–70.
[65] Kwon SC, Adachi T, Araki W, Yamaji A. Thermo-viscoelastic properties of silica particulate-reinforced epoxy composites: considered in terms of the particle packing model. Acta Mater 2006;54:3369–74.
[66] van Hartingsveldt EAA, van Aartsen JJ. Strain-rate dependence of interfacial adhesion in particle-reinforced polymers. Polymer 1991;32:1482–7.
[67] Nicolais L, Guerra G, Migliaresi C, Nicodemo L, Di Benedetto AT. Viscoelastic behavior of glass-reinforced epoxy resin. Polym Compos 1981;2:116–20.
[68] Drozdov AD. Modeling viscoelastic response of particulate polymeric composites with high volume fractions of fillers. Math Comput Model 1999;29:11–25.
[69] Adolf DB, Rchambers OS. Application of a nonlinear viscoelastic model to glassy, particulate-filled polymers. J Polym Sci Part B Polym Phys 2005;43:3135–50.
[70] Nakamura Y, Yamaguchi M, Okubo M, Matsumoto T. Effect of particle size on mechanical properties of epoxy resin filled with angular-shaped silica. J Appl Polym Sci 1992;44:151–8.
[71] Zhang Q, Tian M, Wu Y, Lin G, Zhang L. Effect of particle size on the properties of $Mg(OH)_2$-filled rubber composites. J Appl Polym Sci 2004;94:2341–6.
[72] Lazzeri A, Thio YS, Cohen RE. Volume strain measurements on $CaCO_3$/polypropylene particulate composites: the effect of particle size. J Appl Polym Sci 2004;91:925–35.

[73] Suprapakorn N, Dhamrongvaraporn SS. Effect of $CaCO_3$ on the mechanical and rheological properties of a ring-opening phenolic resin: polybenzoxazine. Polym Compos 1998;19:126–32.
[74] Singh RP, Zhang M, Chan D. Toughening of a brittle thermosetting polymer: effects of reinforcement particle size and volume fraction. J Mater Sci 2002;37:781–8.
[75] Lange FF, Radford KC. Fracture energy of an epoxy composite system. J Mater Sci 1971;6:1197–203.
[76] Ji XL, Jing JK, Jiang BZ. Tensile modulus of polymer nanocomposites. Polym Eng Sci 2002;42:983–93.
[77] Mishra S, Sonawane SH, Singh RP. Studies on characterization of nano $CaCO_3$ prepared by the in situ deposition technique and its application in PP–nano $CaCO_3$ composites. J Polym Sci Part B Polym Phys 2005;43:107–13.
[78] Douce J, Boilot JP, Biteau J, Scodellaro L, Jimenez A. Effect of filler size and surface condition of nano-sized silica particles in polysiloxane coatings. Thin Solid Films 2004;466:114–22.
[79] Dibendetto AT, Wambach AD. The fracture toughness of epoxy–glass bead composites. Int J Polym Mater 1972;1:159–73.
[80] Wang K, Wu J, Ye L, Zeng H. Mechanical properties and toughening mechanisms of polypropylene/barium sulfate composites. Composite Part A 2003;34:1199–205.
[81] Fu SY, Hu X, Yue CY. The flexural modulus of misaligned short fiber reinforced polymers. Compos Sci Technol 1999;59:1533–42.
[82] Fu SY, Lauke B. Strength anisotropy of misaligned short-fibre-reinforced polymers. Compos Sci Technol 1998;58:1961–72.
[83] Fu SY, Lauke B. Effects of fibre length and orientation distributions on the tensile strength of short fibre reinforced polymers. Compos Sci Technol 1996;56:1179–90.
[84] Einstein A. Ueber die von der molekularkinetischen fluessigkeiten suspendierten teilchen. Ann Phys (Leipzig) 1905;17:549–60.
[85] Einstein A. Investigation on theory of Brownian motion. New York: Dover; 1956.
[86] Hsueh CH, Becher PF. Effective viscosity of suspensions of spheres. J Am Ceram Soc 2005;88:1046–9.
[87] Tavman IH. Thermal and mechanical properties of aluminum powder-filled high-density polyethylene composites. J Appl Polym Sci 1996;62:2161–7.
[88] Guth E. Theory of filler reinforcement. J Appl Phys 1945;16:20–5.
[89] Halpin JC. Stiffness and expansion estimates for oriented short fiber composites. J Compos Mater 1969;3:732–4.
[90] Halpin JC, Tsai SW. Effects of environmental factors on composite materials. Technical Report. AFML-TR 67-423; 1969.
[91] Kerner EH. The elastic and thermoelastic properties of composite media. Proc Phys Soc B 1956;69:808–13.
[92] Nielsen LE. Generalized equation for the elastic moduli of composite materials. J Appl Phys 1970;41:4626–7.
[93] Nielsen LE. Dynamic mechanical properties of polymers filled with agglomerated particles. J Polym Sci Polym Phys 1979;17:1897–901.
[94] Lewis TB, Nielsen LE. Dynamic mechanical properties of particulate filled composites. J Appl Polym Sci 1970;14:1449–71.
[95] Mooney M. The viscosity of a concentrated suspension of spherical particles. J Colloid Sci 1951;6:162–70.
[96] Brodnyan JG. The concentration dependence of the Newtonian viscosity of prolate ellipsoids. Trans Soc Rheol 1959;3:61–8.
[97] Fu SY, Hu X, Yue CY. A new model for the transverse modulus of unidirectional fiber composites. J Mater Sci 1998;33:4953–60.
[98] Ma L, Feng XQ, Gao KW, Yu SW. Elastic and plastic analyses of functionally graded elements. Mater Sci Forum 2003;423-425:731–6.
[99] Coran AY. Thermoplastic elastomeric rubber-plastic blends. In: Bhowmick AK, Stephens HL, editors. Handbook of elastomers – new development and technology. New York: Marcel Dekker Inc.; 1988. p. 249–60.
[100] George S, Prasannakumari L, Koshy P, Varughese KT, Thomas S. Tearing behavior of blends of isotactic polypropylene and nitrile rubber: influence of blend ratio, morphology and compatibilizer loading. Mater Lett 1996;26:51–8.
[101] George S, Joseph R, Thomas S, Varughese KT. Blends of isotactic polypropylene and nitrile rubber: morphology, mechanical properties and compatibilization. Polymer 1995;36:4405–16.
[102] Hashin Z, Shtrikman S. On some variational principles in anisotropic and inhomogeneous elasticity. J Mech Phys Solids 1962;10:335–42.
[103] Torquato S. Random heterogeneous materials: microstructure and macroscopic properties. Heidelberg: Springer; 2002.
[104] Counto UJ. Effect of the elastic modulus, creep and creep recovery of concrete. Mag Concr Res 1964;16:129–38.
[105] Ishai O, Cohen IJ. Elastic properties of filled and porous epoxy composites. Int J Mech Sci 1967;9:539–46.
[106] Paul B. Prediction of constants of multiphase materials. Trans Am Inst Min Metall Pet Eng 1960;218:36–41.
[107] Kuo MC, Tsai CM, Huang JC, Chen M. Composites reinforced by nano-sized SiO_2 and Al_2O_3 particulates. Mater Chem Phys 2005;90:185–95.
[108] Young RJ, Maxwell DL, Kinloch AJ. The deformation of hybrid–particulate composites. J Mater Sci 1985;21:380–8.
[109] Lee J, Yee AF. Fracture behavior of glass bead filled epoxies: cleaning process of glass beads. J Appl Polym Sci 2001;79:1371–83.
[110] Fu SY, Xu G, Mai Y-W. On the elastic modulus of hybrid. Particle/short fiber/polymer composites. Composite Part B 2002;33:291–9.
[111] Jayaraman K, Kortschot MT. Correction to the Fukuda–Kawata Young's modulus theory and the Fukuda–Chou strength theory for short fibre-reinforced composite materials. J Mater Sci 1996;31:2059–64.
[112] Vu-Khanh T, Denault J. The effects of injection moulding on the mechanical behaviour of long-fibre reinforced PBT/PET blends. Compos Sci Technol 1991;40:423–35.
[113] Piggott MR. Short fibre polymer composites: a fracture-based theory of fibre reinforcement. J Compos Mater 1994;28:588–606.
[114] Verbeek CJR. The influence of interfacial adhesion, particle size and size distribution on the predicted mechanical properties of particulate thermoplastic composites. Mater Lett 2003;57:1919–24.
[115] Shang SW, Williams JW, Soderholm KJM. Work of adhesion affects the. mechanical properties of silica-filled composites. J Mater Sci 1994;29:2406–16.
[116] Kojima Y, Usuki A, Kawasumi M, Okada A, Kurauchi T, Kamigaito O. Synthesis of nylon 6–clay hybrid by montmorillonite intercalated with-caprolactam. J Polym Sci Part A Polym Chem 1993;31:983–6.
[117] Kojima Y, Usuki A, Kawasumi M, Okada A, Kurauchi T, Kamigaito O. One-pot synthesis of nylon 6–clay hybrid. J Polym Sci Part A Polym Chem 1993;31:1755–8.
[118] Yano K, Usuki A, Okada A, Kurauchi T, Kamigaito O. Synthesis and properties of polyimide–clay hybrid. J Polym Sci Part A Polym Chem 1993;31:2493–8.
[119] Usuki A, Koiwai A, Kojima Y, Kawasumi M, Okada A, Kurauchi T, et al. Migration of antidegradants to the surface in NR and SBR vulcanizates. J Appl Polym Sci 1995;65:119–25.
[120] Feng XQ. Effective elastic moduli of polymer–clay nanocomposites. Chin Sci Bull 2001;46:1130–3.
[121] Takayanagi M, Ogata T, Morikawa M, Kai T. Polymer composites of rigid and flexible molecules: system of wholly aromatic and aliphatic polyamides. J Macromol Sci Phys B 1980;l7:591–615.
[122] Nemat-Nasser S, Hori M. Micromechanics: overall properties of heterogeneous materials. Amsterdam: North-Holland; 1993.
[123] Mori T, Tanaka K. Average stress in matrix and average energy of materials with misfitting inclusions. Acta Metall 1973;21:571–4.
[124] Drozdov AD, Dorfmann A. The stress–strain response and ultimate strength of filled elastomers. Comput Mater Sci 2001;21:395–417.
[125] Manson JA, Sperling LH. Polymer blends and composites. New York: Plenum; 1976.
[126] Christensen RM, Lo KH. Solutions for effective shear properties in three phase sphere and cylinder models. J Mech Phys Solids 1979;27:315–30.

[127] Halpin JC, Kardos JL. Halpin–Tsai equations: a review. Polym Eng Sci 1976;16:344–52.
[128] Alberola ND, Benzarti K, Bas C, Bomal Y. Interface effects in elastomers reinforced by modified precipitated silica. Polym Compos 2001;22:312–25.
[129] Wang GF, Feng XQ, Yu SW, Nan CW. Interface effects on effective elastic moduli of nanocrystalline materials. Mater Sci Eng A 2003;363:1–8.
[130] Colombini D, Hassander H, Karlsson OJ, Maurer FHJ. Influence of the particle size and particle size ratio on the morphology and viscoelastic properties of bimodal hard/soft latex blends. Macromolecules 2004;37:6865–73.
[131] Colombini D, Maurer FHJ. Origin of additional mechanical transitions in multicomponent polymeric materials. Macromolecules 2002;35:5891–902.
[132] Sevostianova I, Kachanov M. Effect of interphase layers on the overall elastic and conductive properties of matrix composites. Applications to nanosize inclusion. Int J Solids Struct 2007;44: 1304–15.
[133] Shen LX, Li J. Effective elastic moduli of composites reinforced by particle or fiber with an inhomogeneous interphase. Int J Solids Struct 2003;40:1393–409.
[134] Lutz MP, Zimmerman RW. Effect of an inhomogeneous interphase zone on the bulk modulus and conductivity of a particulate composite. Int J Solids Struct 2005;42:429–37.
[135] Sharma P, Ganti S. Size-dependent Eshelby's tensor for embedded nano-inclusions incorporating surface/interface energies. J Appl Mech 2004;71:663–71.
[136] Zhong Z, Maguid SA. On the imperfectly bonded spherical inclusion problem. J Appl Mech 1999;66:839–46.
[137] Li HX, Liu YH, Feng XQ, Cen ZZ. Limit analysis of ductile composites based on homogenization theory. Proc R Soc Lond A 2003;459:659–75.
[138] Shi DL, Feng XQ, Huang Y, Hwang KC, Gao H. The effect of nanotube waviness and agglomeration on the elastic property of carbon nanotube-reinforced composites. J Eng Mater Technol 2004;126:250–7.
[139] Feng XQ, Shi DL, Huang Y, Hwang KC. Multiscale mechanics of carbon nanotubes and their composites. In: Sih GC, editor. Multiscaling in molecular and continuum mechanics: interaction of time and size from macro to nano. The Netherlands: Springer; 2007. p. 103–39.
[140] Kontou E. Micromechanics model for particulate composites. Mech Mater 2007;39:702–9.
[141] Rong MZ, Zhang MQ, Pan SL, Lehmann B, Friedrich K. Analysis of the interfacial interactions in polypropylene/silica nanocomposites. Polym Int 2004;53:176–83.
[142] Buggy M, Bradley G, Sullivan A. Polymer–filler interactions in kaolin/nylon 6,6 composites containing a silane coupling agent. Composite Part A 2005;36:437–42.
[143] Nakamura Y, Okabe S, Iida T. Effects of particle shape, size and interfacial adhesion on the fracture strength of silica-filled epoxy resin. Polym Polym Compos 1999;7:177–86.
[144] Packham DE. Work of adhesion: contact angles and contact mechanics. Int J Adhes Adhes 1996;16:121–8.
[145] Creton C, Kramer EJ, Brown HR, Hui CY. Adhesion and fracture of interfaces between immiscible polymers: from the molecular to the continuum scale. Adv Polym Sci 2001;156: 53–136.
[146] Harding PH, Berg JC. The characterization of interfacial strength using single-particle composites. J Adhe Sci Technol 1997;11: 1063–76.
[147] Mower TM, Argon AS. An experimental technique to measure the adhesive and transparent matrices. J Mater Sci 1996;31:1585–94.
[148] Lauke B. Determination of adhesion strength between a coated particle and polymer matrix more composites. Compos Sci Technol 2006;66:3153–60.
[149] Dekkers MEJ, Heikens D. The effect of interfacial adhesion on the mechanism for ... polystyrene–glass bead composites. J Mater Sci 1983;18:3281–7.
[150] Wu CL, Zhang MQ, Rong MZ, Friedrich K. Silica nanoparticles filled polypropylene: effects of particle surface treatment, matrix ductility and particle species on mechanical performance of the composites. Compos Sci Technol 2005;65:635–45.
[151] Thio YS, Argon AS, Cohen RE. Role of interfacial adhesion strength on toughening polypropylene with rigid particles. Polymer 2004;45:3139–47.
[152] Jiang L, Zhang J, Wolcott MP. Comparison of polylactide/nano-sized calcium carbonate and polylactide/montmorillonite composites: reinforcing effects and toughening mechanisms. Polymer 2007;48:7632–44.
[153] Li Y, Fu SY, Lin DJ, Zhang YH, Pan QY. Mechanical properties of polyimide composites filled with SiO_2 nano-particles at room temperature and cryogenic temperatures. Acta Mater Compos Sinica 2005;22:11–5.
[154] Li Y. Cryogenic properties of silica/polyimide hybrid films. Master thesis, Chinese Academy of Sciences, Beijing; 2004.
[155] Maazouz A, Sautereau H, Gerard JF. Hybrid–particulate composites based on an epoxy matrix, a reactive rubber, and glass beads: morphology viscoelastic, and mechanical properties. J Appl Polym Sci 1993;50:615–26.
[156] Chen Y, Zhou S, Yang H, Wu L. Structure and properties of polyurethane/nanosilica composites. J Appl Polym Sci 2005;95: 1032–9.
[157] Nielsen LE. Simple theory of stress–strain properties of filled polymers. J Appl Polym Sci 1966;10:97–103.
[158] Nicolais L, Nicodemo L. Strength of particulate composite. Polym Eng Sci 1973;13:469.
[159] Nicolais L, Narkis M. Stress–strain behaviors of SAN/glass bead composites in the glassy region. Polym Eng Sci 1971;11:194–9.
[160] Jancar J, Dianselmo A, Dibenedetto AT. The yield strength of particulate reinforced thermoplastic composites. Polym Eng Sci 1992;32:1394–9.
[161] Leidner J, Woodhams RT. Strength of polymeric composites containing spherical fillers. J Appl Polym Sci 1974;18:1639–54.
[162] Bigg DM. Mechanical properties of particulate filled polymers. Polym Compos 1987;8:115–22.
[163] Lu S, Yan L, Zhu X, Qi Z. Microdamage and interfacial adhesion in glass bead-filled high-density polyethylene. J Mater Sci 1992;27: 4633–8.
[164] Piggott MR, Leidner J. Misconceptions about filled polymers. J Appl Polym Sci 1974;18:1619–23.
[165] Turcsanyi B, Pukanszky B, Tudos F. Composition dependence of tensile yield stress in filled polymers. J Mater Sci Lett 1988;7:160–2.
[166] Pukanszky B, Turcsanyi B, Tudos F. Effect of interfacial interaction on the tensile yield stress of polymer composites. In: Ishida H, editor. Interfaces in polymer, ceramic and metal matrix composites. Amsterdam: Elsevier; 1988. p. 467–77.
[167] Liang JZ, Li RKY. Prediction of tensile yield strength of rigid inorganic particulate filled thermoplastic composites. J Mater Process Technol 1998;83:127–30.
[168] Landon G, Lewis G, Boden G. The influence of particle size on the tensile strength of particulate-filled polymers. J Mater Sci 1977;12:1605–13.
[169] Hojo H, Toyoshima W, Tamura M, Kawamura N. Short- and long-term strength characteristics of particulate-filled cast epoxy resin. Polym Eng Sci 1974;14:604–9.
[170] Hojo H, Toyoshima W. In: The 31st ANTEC, SPE Montreal, Canada (1973) (Technomic, 1973). p. 163.
[171] Li G, Helms JE, Pang SS, Schulz K. Analytical modeling of tensile strength of particulate filled composites. Polym Compos 2001;22:593–603.
[172] Atkins AG, Mai Y-W. Elastic and plastic fracture. Chichester: Ellis Horwood; 1985 and 1988 editions.

[173] Sih GC, Paris PC, Irwin GR. On cracks in rectilinearly anisotropic bodies. Int J Fract 1965;1:189–203.
[174] Michler GH. Micromechanics of polymers. J Macromol Sci B 1999;38:787–802.
[175] Nakamura Y, Yamaguchi M. Effect of particle size on fracture toughness of epoxy resin filled with angular-shaped silica. Polymer 1991;32:2221–9.
[176] Brown HR. A model for brittle–ductile transitions in polymers. J Mater Sci 1982;17:469–76.
[177] Argon AS, Cohen RE. Toughenability of polymers. Polymer 2003;44:6013–32.
[178] Evans AG, Williams S, Beaumont PWR. On the toughness of particulate filled polymers. J Mater Sci 1985;20:3668–74.
[179] Nakamura Y, Yamaguchi M. Effect of particle size on the fracture toughness of epoxy resin filled with spherical silica. Polymer 1992;33:3415–26.
[180] Zhang L, Li C, Huang R. Toughness mechanism in polypropylene composites: PP toughened with elastomer and calcium carbonate. J Polym Sci Part B Polym Phys 2004;42:1656–62.
[181] Guo T, Wang L, Zhang A, Cai T. Effects of nano calcium carbonate modified by a lanthanum compound on the properties of polypropylene. J Appl Polym Sci 2005;97:1154–60.
[182] Wetzel B, Haupert F, Zhang MQ. Epoxy nanocomposites with high mechanical and tribological performance. Compos Sci Technol 2003;63:2055–67.
[183] Liu ZH, Kwok KW, Li RKY, Choy CL. Effects of coupling agent and morphology on the impact strength of high density polyethylene/$CaCO_3$ composites. Polymer 2002;43:2501–6.
[184] Zuiderduin WCJ, Westzaan C, Huetink J, Gaymans RJ. Toughening of polypropylene with calcium carbonate particles. Polymer 2003;44:261–75.
[185] Maxwell D, Young RJ, Kinloch AJ. Hybrid particulate-filled epoxy-polymers. J Mater Sci Lett 1984;3:9–12.
[186] Pukánszky B, Maurer FHJ. Composition dependence of the fracture toughness of heterogeneous polymer systems. Polymer 1995;36:1617–25.
[187] Gutowski WS. Physical model of interface and interphase performance in composite materials and bonded polymers. Die Angew Makromol Chem 1999;272:51–6.
[188] Hayes BS, Seferis JC. Modification of thermosetting resins and composites through preformed particles. Polym Compos 2004;22:451–67.
[189] Garg AC, Mai Y-W. Failure mechanisms in toughened epoxy resins – a review. Compos Sci Technol 1988;31:179–223.
[190] Friedrich K, Karsch UA. Fatigue crack growth and fracture in glass sphere-filled nylon 6. Polym Compos 1982;3:65–74.
[191] Lee J, Yee AF. Inorganic particle toughening II: toughening mechanisms of glass bead filled epoxies. Polymer 2001;42:589–97.
[192] Lee J, Yee AF. Inorganic particle toughening I: micro-mechanical deformations in the fracture of glass bead filled epoxies. Polymer 2001;42:577–88.
[193] Faber KT, Evans AG. Crack deflection processes – I: theory. Acta Metall 1983;31:565–76.
[194] Azimi HR, Pearson RA, Hertzberg RW. Fatigue of hybrid epoxy composites: epoxies containing rubber and hollow glass spheres. Polym Eng Sci 1996;36:2352–65.
[195] Johnsen BB, Kinloch AJ, Mohammed RD, Taylor AC, Sprenger S. Toughening mechanisms of nanoparticle-modified epoxy polymers. Polymer 2007;48:530–41.
[196] Zhang H, Zhang Z, Friedrich K, Eger C. Property improvements of in situ epoxy nanocomposites with reduced interparticle distance at high nanosilica content. Acta Mater 2006;54:1833–42.
[197] Evans AG. The strength of brittle materials containing second phase dispersions. Philos Mag 1972;26:1327–44.
[198] Green DJ, Nicholson PS, Embury JD. Fracture of a brittle particulate composite, part 1: experimental aspects. J Mater Sci 1979;14:1413–20.
[199] Green DJ, Nicholson PS, Embury JD. Fracture of a brittle particulate composite, part 2: theoretical aspects. J Mater Sci 1979;14:1657–61.
[200] Phipps MA, Pritchard G, Abou-Torabi A. Role of particle strength and filler volume fraction in the fracture of alumina trihydrate filled epoxy resins. Polym Polym Compos 1995;3:71–7.
[201] Evans AG, Graham LJ. A model for crack propagation in polycrystalline ceramics. Acta Met 1975;23:1303–12.
[202] Moloney AC, Kausch HH, Stieger HR. The fracture of particulate-filled epoxide resins. J Mater Sci 1983;18:208–16.
[203] Lange FF. Fracture energy and strength behavior of a sodium borosilicate glass–Al_2O_3 composite system. J Am Ceram Soc 1971;54:614–20.
[204] Mallick PK, Broutman L. Mechanical and fracture behavior of glass bead filled epoxy composites. J Mater Sci Eng 1975;18:63–73.
[205] Green DJ, Nicholson PS. Studies in brittle porous materials. J Mater Sci 1977;12:987–9.
[206] Gao H, Rice JR. Somewhat circular tensile cracks. Int J Fract 1987;33:155–74.
[207] Rice JR, Ben-Zion Y, Kim K. Three-dimensional perturbation solution for a dynamic planar crack moving unsteadily in a model elastic solid. J Mech Phys Solids 1994;42:813–43.
[208] Perrin G, Rice JR. Disordering of dynamic planar crack front in a model elastic medium of random variable toughness. J Mech Phys Solids 1994;42:1047–64.
[209] Low IM, Mai Y-W. Rate and temperature effects on crack blunting mechanisms in pure and modified epoxies. J Mater Sci 1989;24:1634–44.
[210] Low IM, Mai Y-W. Micromechanisms of crack extension in unmodified and modified epoxy resins. Compos Sci Technol 1988;33:191–212.
[211] Kinloch AJ, Williams JG. Crack blunting mechanisms in polymers. J Mater Sci 1980;15:987–96.
[212] Feng XQ, Yu SW. Damage mechanics. Beijing: Tsinghua University Press; 1997.
[213] Lemaitre J. A course on damage mechanics. Berlin: Springer-Verlag; 1992.
[214] Bucknall CB. Fracture and failure of multiphase polymers and polymer composites. Adv Polym Sci 1978;27:121–48.
[215] Ishai O, Cohen LJ. Effect of fillers and voids on compressive yield of epoxy composites. J Compos Mater 1968;2:302–26.
[216] Zebarjad SM, Tahani M, Sajjadi SA. Influence of filler particles on deformation and fracture mechanism of isotactic polypropylene. J Mater Proc Technol 2004;155-156:1459–64.
[217] Friedrich K, Karsch UA. Failure processes in particulate filled polypropylene. J Mater Sci 1981;16:2167–79.
[218] Evans AG, Ahmad ZB, Gilbert DG, Beaumont PWR. Mechanisms of toughening in rubber toughened polymers. Acta Metall 1986;34:79–87.
[219] Bohse J, Grellmann W, Seidler S. Micromechanical interpretation of fracture toughness of particulate-filled thermoplastics. J Mater Sci 1991;26:6715–21.
[220] Fekete E, Molnar S, Kim GM, Michler GH, Pukanszky B. J Macromol Sci B 1999;38:885–99.
[221] Argon AS, Bartczak Z, Cohen RE, Muratoglu OK. Novel mechanisms of toughening semi-crystalline polymers. In: Pearson RA, Sue HJ, Yee AF, editors. Toughening of plastics: advances in modeling and experiments. Modeling and experiments symposium series 759. Washington, DC: ACS; 2000. p. 98–124.
[222] Bartczak Z, Argon AS, Cohen RE, Weinberg M. Toughness mechanism in semi-crystalline polymer blends: I. High-density polyethylene toughened with rubbers. Polymer 1999;40:2331–46.
[223] Wilbrink MWL, Argon AS, Cohen RE, Weinberg M. Toughenability of nylon-6 with $CaCO_3$ filler particles: new findings and general principles. Polymer 2001;42:10155–80.
[224] Martuscelli E, Musto P, Ragosta G. Advanced routes for polymer toughening. Amsterdam: Elsevier; 1996.

[225] Wu S. Phase structure and adhesion in polymer blends: a criterion for rubber toughening. Polymer 1985;26:1855–63.
[226] Wu S. A generalized criterion for rubber toughening: the critical matrix ligament thickness. J Appl Polym Sci 1988;35:549–61.
[227] Muratoglu OK, Argon AS, Cohen RE, Weinberg M. Toughening mechanism of rubber-modified polyamides. Polymer 1995;36: 921–30.
[228] Bartczak Z, Argon AS, Cohen RE, Cohen KT, Kowalewski T. The morphology and orientation of polyethylene in films of sub-micron thickness crystallized in contact with calcite and rubber substrates. Polymer 1999;40:2367–80.
[229] Dasari A, Yu ZZ, Mai Y-W. Transcrystalline regions in the vicinity of nanofillers in polyamide-6. Macromolecules 2007;40:123–30.